

OPTICAL SPECTROSCOPY OF URU₂SI₂:
A SEARCH FOR NEW FEATURES

OPTICAL SPECTROSCOPY OF URU_2Si_2 :
A SEARCH FOR NEW FEATURES

By

SARAH PURDY, B.Sc.

A Thesis
Submitted to the School of Graduate Studies
in Partial Fulfilment of the Requirements
for the Degree
Master of Science

McMaster University
© Copyright by Sarah Purdy

MASTER OF SCIENCE (2010)
(Physics and Astronomy)

McMaster University
Hamilton, Ontario

TITLE: Optical Spectroscopy of URu_2Si_2 :
A Search for New Features

AUTHOR: Sarah Purdy
B. Sc., 2007 (Trent University, Canada)

SUPERVISOR: Professor T. Timusk

NUMBER OF PAGES: ix, 87

Abstract

In the past, optical measurements of single crystals have provided insights into phase transitions, the structure and symmetry of the superconducting gap and many other phenomena. Competing groups are perpetually trying to improve the accuracy of measurements to contribute to the understanding of the materials they study. Recent improvements at McMaster included the installation of a translating stage that allowed for submillimeter control of sample position, the measurement of several samples in one experiment, and measurements at temperatures of 10 - 300 K. The stage was attached to an external sample chamber on a spectrometer that can be used to measure frequencies from 20 to 38,000 cm^{-1} . The new sample stage was used in measurements of the reflectance spectra of a single crystal URu_2Si_2 sample. The reflectance measurements were used to calculate the absolute reflectance and optical conductivity.

It was observed that for temperatures below 50 K at frequencies below 100 cm^{-1} , the reflectance appeared to have a parabolic trend. A linear regression was used to fit the absolute reflectance measured by Dr. Nagel (2010) in order to determine the numeric values of the parabolic model with the best fit data. The regression gave the optimized equation: $P = 0.9872 - 8.0279\text{E-}6*\omega^2$ with a regression coefficient of 0.8417. This showed that over 84% of the variability in the data was accounted for by the model. This model was used to calculate the absolute reflectance from the thermal reflectance data at 3 K collected by Dr. Nagel (2010) and was shown to have a standard deviation of ± 0.011 . The result was called the “refined” absolute reflectance, and the refining method was repeated on the thermal reflectance measurements conducted by Dr. Nagel’s group.

The ω^2 behaviour was attributed to electron-electron interaction described by Fermi Liquid Theory. The strength of the electron-electron interaction was calculated to be $A = 0.26 \mu\Omega\text{cmK}^{-2}$ using dc resistivity data from Levallois *et al.* (2009). The optical conductivity data from Dr. Lobo (2010), as well as the results calculated from the refined absolute reflectance and from the measurements made using our new spectrometer system, were used to determine A as 0.21, 0.23, and 0.23 $\mu\Omega\text{cmK}^{-2}$ respectively.

Acknowledgements

I would like to express my deepest gratitude to my advisor Tom Timusk for the opportunity to work in his research group. I'd like to thank him for his patient guidance, and for sharing his anecdotes and expertise. I am most deeply thankful for his understanding and consideration, and especially his support. He has provided me with many opportunities to attend workshops and conferences, and was a great encouragement during my presentations.

I would also like to express my deepest appreciation to Jules Carbotte for his kind encouragement and discussions. My conversations with him were a great resource for all of my presentations and work. I would like to thank Jules and Ewald Schachinger for providing the modelled conductivity gap models for this thesis and other presentations.

I would like to thank my group mates for their hard work: Jesse Hall, Alison Kinross, Jungseek Hwang, Jinshan Zhang, Greg Egan, and Jing Yang. Thanks also to Graeme Luke, Travis Williams and Jim Garrett for growing the samples used in this thesis, and extended thanks to Jim for all of his helpful advice and 'you-know-what-you-could-do's. His problem solving and numerous supplies were very helpful in completing many repairs and modifications to the equipment I used.

I gratefully acknowledge Urmas Nagel and Toomas Rõõm for sharing their beautiful results and allowing me to use their data in my thesis.

Finally, I'd like to thank the friends and family that have been alongside me these past two years. Thanks to friends, Ray Ng, James Leblanc, Travis Williams and Jerod Wagman, for their tutoring and kind words. Thanks especially to Jesse and Krista

Hall for breakfast and perspective. Thanks to my sisters, Serena and Courtney for their support, and advice over the years. I deeply appreciate the subtle support of my partner Troy. Last but not least, my most humble thanks to my parents for their love, encouragement and support over all of the years. Their wisdom and guidance was crucial to my success.

*Hamilton, Ontario
August, 2010*

Sarah Purdy

Table of Contents

1 Introduction	1
1.1 Motivation.....	2
1.2 Thesis Outline.....	4
2 Optical Spectroscopy.....	5
2.1 Spectrometer.....	5
2.2 Reflectance Ratios	7
2.3 Absolute Reflectance.....	11
3 Measurement System	13
3.1 Sample Preparation.....	15
3.2 Sample mounting	17
3.3 Sample alignment	20
3.4 Sample Cooling.....	23
3.5 Sample Chamber and Motorized Translating Stage.....	26
3.6 Evaporation Chamber	32
3.7 Detector Preparation and Acquiring a Signal.....	38
3.7.1 1 K and 4 K Bolometers.....	38
3.7.2 Mercury-Cadmium-Telluride (MCT) Detector.....	46
3.7.3 Photomultiplier Tube (PMT)	47
3.7.4 Data Acquisition Software.....	48
4 Measurement Procedure.....	50
4.1 Measurement Procedure for the FIR, MIR and NIR Spectral Ranges.....	52
4.2 Measurement Procedure for the VIS/UV Spectral Region.....	56
5 Data Analysis	58
5.1 Thermal Reflectance and Refinement of the Absolute Reflectance at Low Frequencies	58
5.2 Absolute Reflectance.....	69
5.3 Optical Conductivity.....	72
5.4 Fermi Liquid Behaviour	75
6 Conclusion and Continued Work.....	78
Appendix A: Bruker Run Checklist.....	83
Appendix B: Cleaving layered materials.....	86

List of Figures and Tables

Figure 1 Optical conductivity adapted from Fig. 11, Degiorgi <i>et al.</i> , 1997.....	2
Figure 2 Reflectance ratio from collaborators in Paris (Lobo, 2010).	3
Figure 3: Sketch of spectrometer with light path.....	7
Figure 4 Transmittance ratio for metallic lead. (Palmer and Tinkham, 1968).....	8
Figure 5 Model of a single s-wave gap (dot-dash line), compared to a single s+d-wave gap (Carbotte and Schachinger, 2010).....	9
Figure 6 Model thermal reflectance ($t=T/T_c$) of a single d-wave gap at a variety of temperatures (Carbotte and Schachinger, 2010).	10
Figure 7 Features observed using optical spectroscopy (Basov and Timusk, 2005)	12
Figure 8 Illustration of sample holder and alignment.	22
Figure 9 Cryostat cold finger with three samples mounted	24
Figure 10 Complete spectrometer system with helium Dewar and transfer line.....	26
Figure 11 McAllister stage showing jacking screws and gear system, and bellows	28
Figure 12 Sample box.	29
Figure 13 Window block	30
Figure 14 Evaporator box.	33
Figure 15 Evaporator plate with filaments and leads attached	35
Figure 16 Complete sample chamber assembly.....	37
Figure 17 Bolometer nozzles for liquid helium transfer and vacuum pump	45
Figure 18 Thermal reflectance of URu ₂ Si ₂ measured in Hamilton, Canada.....	60
Figure 19 Thermal reflectance of URu ₂ Si ₂ (Nagel, 2010).	61

Figure 20 Absolute reflectance at 20 K (Nagel, 2010) plotted against frequency-squared for linear regression.	63
Figure 21 Parabolic fit to 20 K absolute reflectance from Tallinn (Nagel, U., 2010)	64
Figure 22 Absolute Reflectance and Refined Reflectance at 3 K.....	65
Figure 23 Refined absolute reflectance.....	67
Figure 24 Optical conductivity calculated using the refined absolute reflectance	68
Figure 25 Absolute reflectance URu_2Si_2	70
Figure 26 URu_2Si_2 Optical conductivity	74
Figure 27 DC resistivity at zero magnetic field and at $B = 50$ T (Levallois <i>et al.</i> , 2009) ..	76
Table 1 Spectrometer setup and components.....	14
Table 2 Settings, coating material and OPUS program used for each spectral range.....	15
Table 3 Temperature steps taken for each spectral range.	51
Table 4 Fermi liquid parameter calculated using optical conductivity	77

1 Introduction

Reflectance spectra can be used to examine properties of a material that involve the absorption of light. For example, in superconductors light is absorbed by charge carriers that gain enough energy to overcome the superconducting gap and retain the energy. Besides the superconducting gap, reflectance measurements can be used to examine the scattering rate, neutron resonance, phonons, and electronic transitions (Basov and Timusk, 2005). Improvements to equipment used to measure the reflectance of a sample can help to improve the signal to noise and accuracy of the measurements, which lead to new developments in the understanding of the material. Using a new translating sample stage, a single crystal of URu_2Si_2 was measured to higher accuracy than in an earlier optical study done at McMaster (Bonn *et al.*, 1988). The work done in 1988 showed that the absolute reflectance exhibited the behaviour of a metal with strong magnetic scattering, with a transition to coherent behaviour at $T_c = 70$ K, and provided evidence of an energy gap known as a hidden order (HO) transition at 46 to 61 cm^{-1} below 17.5 K.

1.1 Motivation

URu₂Si₂ has been a material of interest for over 23 years (Palstra *et al.*, 1985). It undergoes a phase transition at 17.5 K that has not been explained since its discovery (Palstra *et al.*, 1986). As techniques and equipment improve, this material is revisited in order to more thoroughly investigate this HO transition. A review of optical studies of URu₂Si₂ show a few interesting features that warranted further investigation. In 1997, Degiorgi *et al.* published optical conductivity data shown in Figure 1. As temperature decreases, the peak in the conductivity near 50 cm⁻¹ was shown to change in frequency.

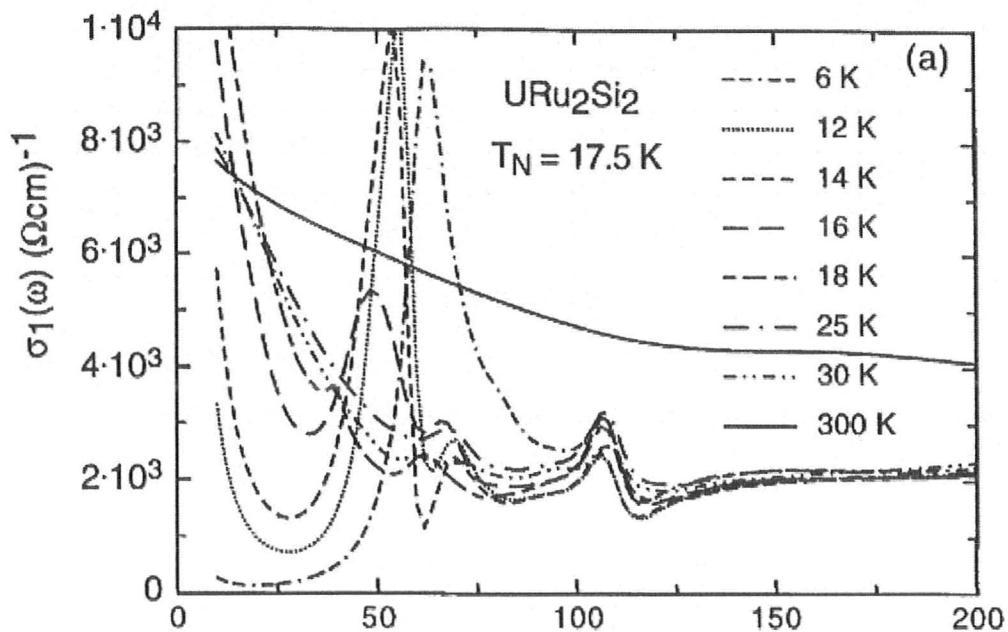


Figure 1 Optical conductivity adapted from Fig. 11, Degiorgi *et al.*, 1997.

Interest was also raised by optical data received from collaborators in Paris led by Dr. Lobo (Lobo, 2010). In Figure 2 the thermal reflectance calculated using the data from Paris seems to indicate two additional features near the HO gap indicated by arrows.

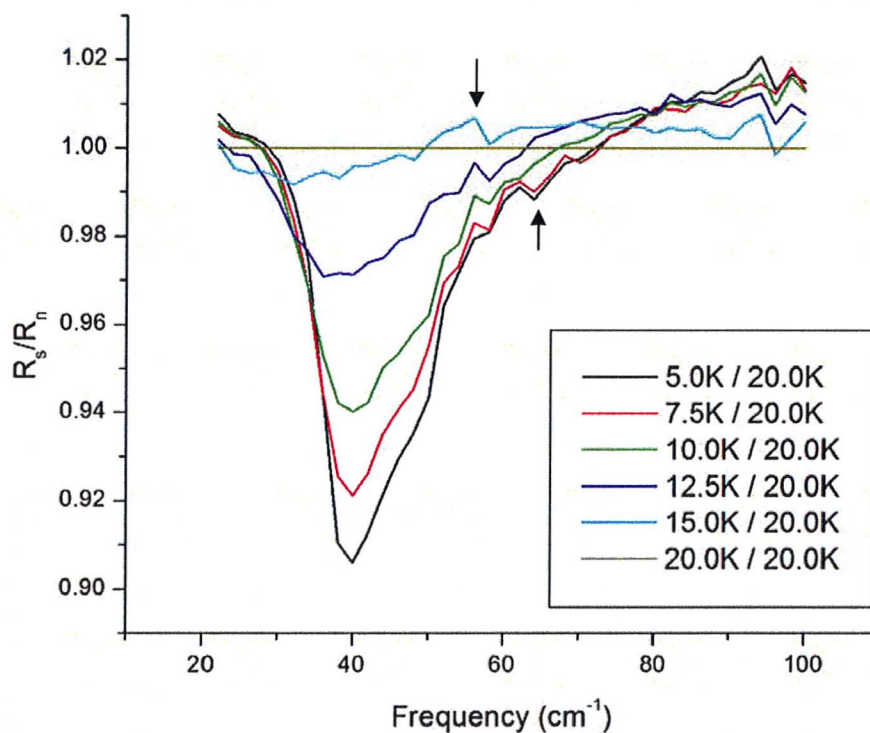


Figure 2 Reflectance ratio from collaborators in Paris (Lobo, 2010).
Note the extra features indicated by arrows.

Using the recently improved spectrometer at McMaster the intent in this thesis was to measure undoped URu_2Si_2 with high accuracy in order to further investigate the HO transition and these associated features.

1.2 Thesis Outline

This thesis contains 6 Chapters, including the introduction. Chapter 2 provides an overview of optical spectroscopy, and a discussion of the measurements (thermal and absolute reflectance) that are used as the foundation for analysis of optical properties as well as features and energy gaps associated with phase transitions in a material. The equipment used for the measurements conducted for this thesis is discussed, in detail, in Chapter 3. The method that was used in the experiments is outlined in Chapter 4, including discussion of the *in situ* evaporation technique for coating samples with metal to correct for surface imperfections. This technique was pioneered by the Timusk group (Homes *et al.*, 1993). The results of the measurements of the URu₂Si₂ sample are reported in Chapter 5, including the thermal reflectance, absolute reflectance, and optical conductivity. Reflectance data collected by Dr. Nagel (2010) at the National Institute of Chemical Physics and Biophysics, in Tallinn, Estonia, was used to test a curve smoothing technique. This curve smoothing or refinement method was used to improve the absolute reflectance provided by Dr. Nagel, which was further used to calculate the optical conductivity in the 10 – 200 cm⁻¹ spectral range, between 3 and 25 K. The conclusions of the measurements and analysis done using the new sample stage with the spectrometer system in the Timusk lab at McMaster, and the results of the refinement method are summarized in Chapter 6.

2 Optical Spectroscopy

2.1 Spectrometer

The optical reflectance measurements were carried out using a commercial Bruker IFS 66v/S FTIR spectrometer. This spectrometer had an operating range from 20 to 40,000 cm^{-1} covering the ultraviolet (UV), visible (VIS), mid-infrared (MIR), near-infrared (NIR) and far-infrared (FIR) frequency ranges. The system was made up of two parts, a Michelson type interferometer and a light chamber that collected reflected light from the external sample chamber and directed it to an external detector. The Bruker had holders for two light sources, which could be removed if different light sources were required. A SiC globar, Hg arc lamp, tungsten and deuterium (D_2) lamp were used for measurements on a URu_2Si_2 sample. The relevant ranges and equipment combinations used are discussed in Chapter 3. The light path is illustrated in Figure 3. Light from the desired source is collected by a concave mirror and passes through an aperture wheel. Sizes 4 and 6 mm were chosen for the measurements on URu_2Si_2 , the beam size was selected to “overfill” the sample area for all of the samples mounted on the cryostat. The mirror and aperture wheel were connected to small stepper motors that allowed for computer controlled selection of light source and aperture size. The control software is described in Chapter 3. The light passed through the

selected aperture and hit a second concave mirror that redirected it through a beam splitter that was oriented at a 45° angle to the beam, half of the light was passed through the beam splitter and half was reflected. The reflected part of the beam was again reflected by a fixed plane mirror back toward the beam splitter and half of that beam passed through. The transmitted beam hit a plane mirror on a travelling stage and was reflected back to the beam splitter where half of it was reflected 90° and combined with the transmitted beam from the fixed plane mirror. Changing the position of the travelling mirror induced a path difference in the two beams which was responsible for a phase difference between the transmitted and reflected beams. In general, for a single wavelength a phase difference results in a change in intensity as the two beams move in and out of phase, for multiple wavelengths the result is an interference pattern. A Fourier transform on the interferogram results in a number of frequency and intensity values that are then used to plot a spectrum: light intensity plotted against light frequency. Changing the position of the mirror on the translating stage allowed a range of frequencies to be measured. The motion of the mirror from one end of the stage to the other, and the measurements collected in that time were called a “scan,” several scans were averaged to reduce the noise in the spectra and improve the accuracy of the data.

The beam from the interferometer was directed into the light chamber using three fixed plane mirrors that redirected the light so that it could be focused by a concave mirror through a window to the external sample chamber. The beam

was reflected by the sample back through the window to a concave collection mirror. The collection mirror focused the reflected beam onto an external detector. The light source, beam splitter, window and detectors were chosen based on their operating frequencies, and the characteristic absorption peaks of the materials in each device. Using various combinations of relevant equipment the frequency range that could be measured was $20 - 40,000 \text{ cm}^{-1}$.

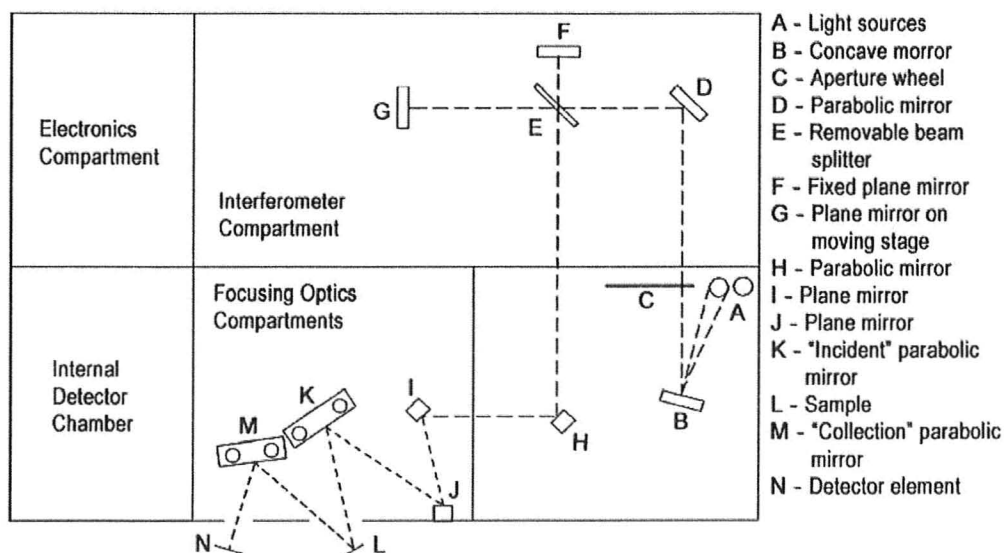


Figure 3: Sketch of spectrometer with light path

2.2 Reflectance Ratios

Optical spectroscopy has been used to determine properties of a material such as the superconducting gap. The ratio of reflectance or transmittance spectra above and below a critical point highlights the energy gap associated with a phase

transition, as shown by Palmer and Tinkham, Phys. Rev. **165**, 588 (1968), in Figure 4.

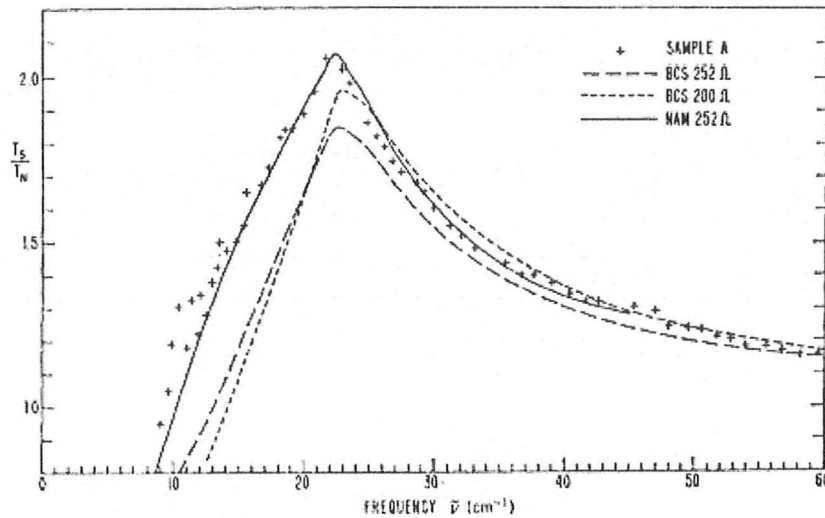


Figure 4 Transmittance ratio for metallic lead. (Palmer and Tinkham, 1968)
Ratio of transmittance spectrum below $T_c = 7$ K to transmittance spectrum above 7 K

This method works especially well for superconductors that have an isotropic or “s-wave” gap and only in the “dirty” limit where the scattering rate of the material is much larger than the gap. In these cases, the peak in the ratio indicates the value of the energy gap at 2Δ which can be compared to results from other methods. For materials that have an anisotropic gap, the ratio does not indicate the value of the energy gap associated with a phase transition, but can be used to identify the symmetry of the gap and other features. For an “extended s-wave” gap, that is an s-wave gap that has some anisotropy, the ratio differs from the ratio for a pure s-wave gap, is shown in Figure 5, kindly provided by Dr.

Carbotte and Dr. Schachinger (2010). For a gap that has more pronounced anisotropy, such as a d-wave gap, the reflectance ratio has a different structure compared to an s-wave or an extended s-wave gap, shown in Figure 5.

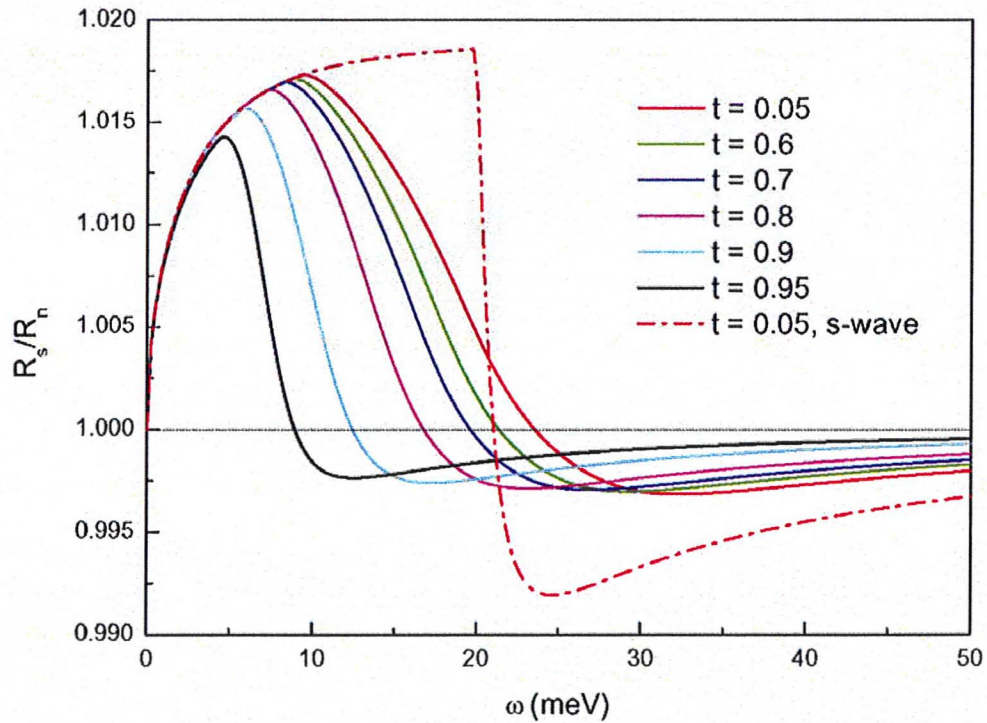


Figure 5 Model of a single s-wave gap (dot-dash line), compared to a single s+d-wave gap (Carbotte and Schachinger, 2010).

A variety of temperatures $t=T/T_c$ are shown, where T_c is the critical temperature in the model.

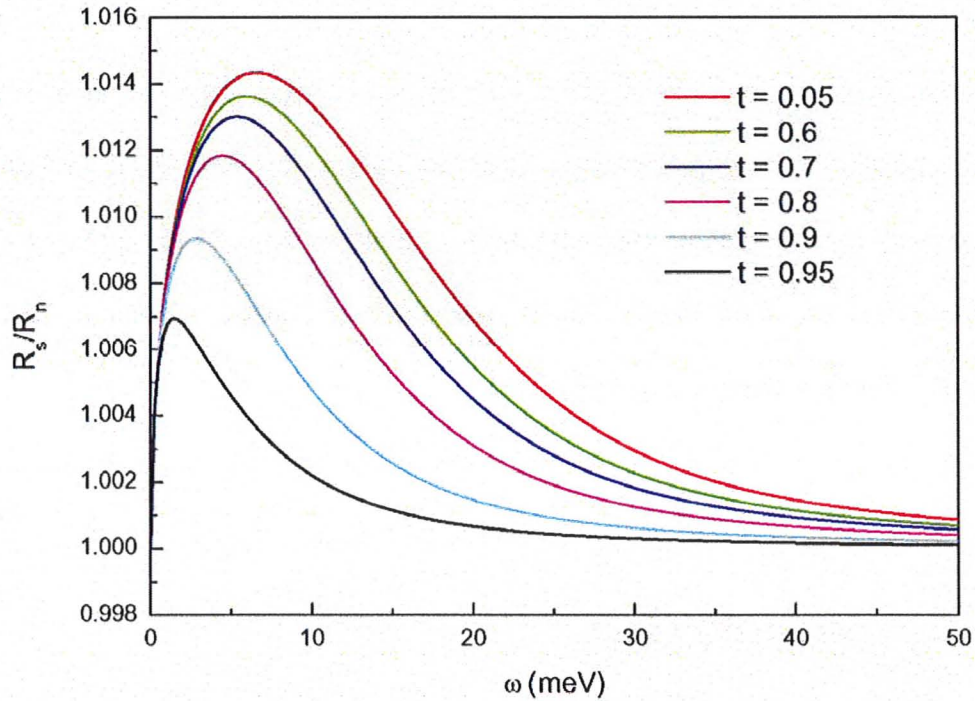


Figure 6 Model thermal reflectance ($t=T/T_c$) of a single d-wave gap at a variety of temperatures (Carbotte and Schachinger, 2010).

For a d-wave superconductor the peak in the thermal reflectance would not indicate the gap value, 2Δ .

Examining the reflectance ratios of a material can provide information about the symmetry and size of an energy gap. For example, the presence of additional peaks in the ratio would be an indication of a second energy gap.

It is important to distinguish between the nomenclature for gap isotropies and atomic orbitals: the two are only related in geometry. An s-wave gap looks like an s orbital - spherical, a d-wave gap looks nodal in the same way that a d orbital has nodes.

A single crystal sample of URu_2Si_2 was grown at McMaster and sent to Dr. Nagel Tallinn, Estonia. The reflectance ratios from 5 to 200 cm^{-1} were

measured between 3 and 20 K and the absolute reflectance was measured at 3 K. A Martin-Puplett spectrometer and 0.3 K bolometer were used to make these measurements. The sample chamber and bolometer were immersed in liquid helium both for cryogenics and isolation from ambient noise. The results of the measurements provided by Dr. Nagel were used to explore a noise reducing analysis technique discussed in Chapter 5.

2.3 Absolute Reflectance

The reflectance of a sample is the spectrum collected using the spectrometer from the light that is reflected by the sample. The spectra measured during the experiments on the URu_2Si_2 sample were corrected using an *in situ* evaporation technique that deposited a thin film of metal onto the reflecting surface. The resulting spectra were used to correct for surface irregularities (Homes *et al.*, 1993), and the corrected data was called the absolute reflectance. Peaks and absorptions in the absolute reflectance spectra, and temperature dependent changes in the spectra can be attributed to a variety of features and properties of the sample, see Figure 7 for a table of such features and the energies at which they are observed. Reflectance measurements can be used to calculate properties of a material such as the scattering rate, optical conductivity and optical constants. The details of these calculations are outlined in Chapter 5.

In the work reported in this thesis, reflectance measurements were performed on a single crystal URu_2Si_2 sample, grown at McMaster by the Luke group, with a frequency range of $20 - 38000 \text{ cm}^{-1}$ and at temperatures between 10 and 300 K.

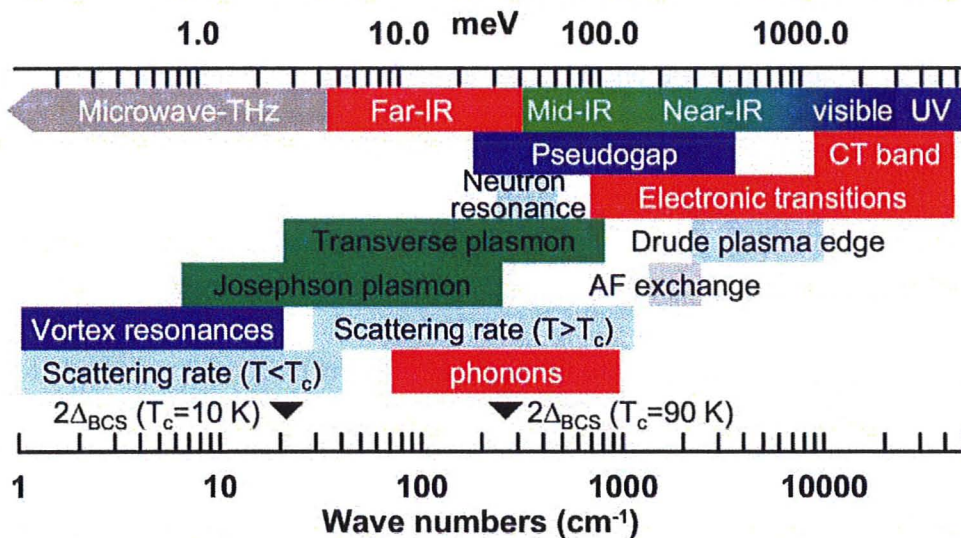


Figure 7 Features observed using optical spectroscopy (Basov and Timusk, 2005)

Shown here is a representation of the energy scales of a variety of phenomena. The pseudogap, electronic transitions, the Drude plasma edge, scattering rate and phonons are some of the things that can be measured in the FIR to UV energy range that is observed using optical techniques,

3 Measurement System

This section covers the equipment and methods used during an experiment. These are outlined in the order of the procedure, accompanied by common problems that are encountered at each step and their solutions. For an abridged version that can be used as a checklist for the experiment see Appendix A.

The complete range of frequencies available from the spectrometer was required to perform Kramers-Kronig analysis of reflectance measurements for the URu_2Si_2 crystal. Using a variety of accessories and components with the Bruker spectrometer, shown in Tables 1 and 2, five sets of data were taken and combined to produce a reflectance spectrum. The frequency ranges that were not measured directly were extrapolated as outlined in Chapter 5.

Taking reflectance measurements of any sample requires that the sample be mounted onto a sample holder, and optically aligned so that the reflected light can be properly focused onto the detector element. The sample chamber and spectrometer were evacuated to reduce risk of ice forming on the sample and to thermally isolate the low temperature sample probe. The vacuum also helps to increase signal amplitude by reducing absorption by atmospheric lines. Spectra were recorded at temperatures between 10 and 300 K and then repeated at the

same or similar temperatures after coating with gold or aluminum. The metal coating was applied using an *in situ* evaporation technique. A gold coating was used for the FIR, MIR and NIR ranges, and aluminum was used for the NIR, VIS and UV ranges.

Frequency (cm^{-1})	Detector	Light Source	Beam Splitter	Window
25-235 (FIR)	1K bolometer	Hg arc lamp	6 μm and 50 μm Ge coated Mylar	Polypropylene
35-600 (FIR)	4K bolometer	Hg arc lamp	6 μm and 50 μm Ge coated Mylar	Polypropylene
450-6,000 (MIR)	77K MCT	SiC Globar	Ge coated KBr	KBr
3,000-14,000 (NIR)	77K MCT	Tungsten	CaF ₂	KBr
13,000-38,000 (VIS/UV)	PMT	D ₂ Lamp	CaF ₂	KBr

Table 1 Spectrometer setup and components

The changeable components for the spectrometer were chosen based on their spectra, so that no absorption lines would interfere with the spectra being measured in each frequency range.

Frequency (cm^{-1})	Filter Settings	Gain Settings	Evaporated Coating	Measurement Program
25-235 (FIR)	0.03, 1k	1000x	Au	BOLO1K.XPM
35-600 (FIR)	0.03, 1k	1000x	Au	BOLLO4KH.XPM
400-6,000 (MIR)	3, 30k	2x	Au	KBRMCT.XPM
3,000-14,000 (NIR)	30k, 100k	2x	Au	QWMCT.XPM
13,000-38,000 (VIS/UV)	300, 300k	100x	Al	D2PMT.XPM

Table 2 Settings, coating material and OPUS program used for each spectral range

The settings and programs required for each frequency range changed depending on the components being used and the frequency range being measured.

3.1 Sample Preparation

The samples were grown by the Luke group at McMaster using the Czochralski technique. U, Ru and Si reagents were pre-melted, cleaned and weighed. The prepared reagents were placed on a water cooled hearth for an arc furnace, enclosed in a bell jar, where they were reacted and homogenized in 1 atm of argon to form a pellet. The reacted pellet was moved to the hearth of a water-cooled tri-arc furnace. The hearth was rotated at 2 Hz and a seed rod was rotated

at 0.5 to 0.75 Hz in the same direction, the crystal grew at an average of 1.5 inches/hour.

The crystal was received with a cleaved face perpendicular to the c-axis. In general, for harder materials, crystals can be cleaved by using a temporary adhesive such as five-minute epoxy, to hold the sample stationary at the correct orientation. It is easier if the sample can be glued to the inside of a 90° corner or L-bracket so that the cleavage plane is flush with the vertical wall of the bracket. The vertical wall of the brace then also serves as a guide for the razor used to cleave the crystal and to ensure that the razor is accurately aligned with the cleavage plane. Spacers may be inserted between the brace and the razor to adjust the thickness of the sample, which will then be the width of the spacers plus half the width of the razor. Before cleaving, the crystal or cleaving system should be covered with a Kim-wipe to avoid loss of any pieces that come off during the process. With the razor held against the sample at the point to be cleaved, and oriented parallel to the cleavage plane, tap the top of the razor with a hammer (only a small amount of force is necessary). The process can be repeated on the same crystal as necessary to achieve flat and parallel faces. The adhesive can be removed using acetone or by heating the brace on a hotplate until the epoxy softens and the sample can be removed using tweezers. For layered materials that are sensitive to moisture an alternative cleaving method is outlined in Appendix B.

3.2 Sample Mounting

The sample was mounted on a brass holder that had a cone shaped face using a small amount of five-minute epoxy. Brass was used for the sample holder because was it easy to work with in machining the cone to fit the sample.

As a general practice, if a sample is very thin or otherwise needs support a substrate which can be cut to size and glued to the sample using a very small amount of five-minute epoxy. Thin brass sheeting is used to make the substrate. A piece of brass sheet is cleaned using sandpaper followed by an acetone wash, and cut using a stainless steel surgical scalpel. Cutting with scissors or stronger cutters will warp the edges of the brass, especially with the small dimensions necessary (1 – 6 mm). Using a sharp scalpel also allows the fine adjustments to be made, although with caution since pressure at the edge of the substrate may also cause warping. Always use a fresh blade! The sample is measured, and the measurements are marked onto the brass sheet. The tip of the scalpel is held to the inside of the mark so that the substrate is made slightly smaller than the sample. Pressure is applied until the scalpel punctures the sheet. The process is repeated, making small cuts each time. “Snipping” along in this fashion is the easiest way to make a cut. If the size of the brass piece needs to be reduced along one edge, holding the whole blade along the edge and pressing the blade downward will take off fractions of a millimetre; rolling the pressure along the curved edge of the

scalpel blade helps avoid bending the brass. The substrate should be the same size or smaller than the sample, since any light that hits the substrate could be reflected back into the light chamber, creating an artefact signal. Once the sample is glued to the substrate the glue should be allowed to set before attempting to glue the combined sample and substrate to the sample holder cone.

The sample cone was custom machined from a 2.54 cm diameter brass rod to have a flat surface at the narrow end to match the size of the sample (3 mm). This maximized the surface area available for thermal contact. In order to avoid the reflection of light from the sample holder into the light chamber of the spectrometer, the surface made on the sample holder was no larger than the sample. The sample itself was an irregular shape 3.3 x 5 mm at its widest points. The face of the cone was 105° from the normal of the crystal surface so that any light that reflected from the cone was deflected by 30° , away from the sample window.

Before mounting the crystal on the sample cone, the crystal was examined to determine the best side or face to measure. The selected face was placed downward on a sheet of waxed paper and set aside. The cone surface was cleaned with acetone or alcohol, and set aside. Five-minute epoxy was mixed on a separate piece of waxed paper. A clean toothpick was dipped into the epoxy and dabbed on a clean part of the waxed paper to remove excess epoxy. A small amount of epoxy was applied to the sample surface of the cone, and then the cone was held upside down over the sample and lowered so that the epoxy of the cone

touched the back of the sample. The epoxy on the cone formed a bond with the sample and the cone was turned right side up. While the epoxy was still soft, a pair of plastic tweezers or a toothpick was used to center the sample on the cone, ensuring that nothing of the flat sample surface of the cone was showing. The centering was done under a microscope.

It was important for the surface of the sample to be parallel with the back of the cone as this made alignment on the multi-sample supporting stage of the cryostat easier. A sample that is at an angle to the cone may require the cone to be tilted at such an angle on the cold finger of the cryostat that it leans against its neighbour and there may not be enough clearance remaining for accurate alignment. This would necessitate re-mounting the sample on the cone. Care was taken not to apply too much epoxy on the cone, because it can squeeze around the sides of the crystal and can get on the face of the crystal when attaching the sample to the cone; it can also get on the tools being used to manipulate the crystal. (Some samples that are tolerant to humidity and solvent can be washed with acetone to remove the epoxy from the face, but samples like $\text{Ba}(\text{Fe}_{1-x}\text{Co}_x)_2\text{As}_2$ would be unusable if epoxy gets on the surface. See Appendix B for a cleaving method that allows for the removal of the top layers of a sample contaminated with glue and recovery of a surface that can be measured).

The sample holder cones for a spectroscopy run were connected to the cryostat cold finger using four fastening screws and two set-screws allowing for a small amount of adjustment in the angle of the face of the sample, as shown in

Figure 8. The cryostat had threaded holes for up to four cones, allowing for three samples and one stainless steel, or gold, reference mirror held in a vertical column (seen in Figure 9) when the cryostat was placed in the sample chamber. Two other samples of different materials were attached to the cryostat with the URu_2Si_2 sample for all of the experiments so that three sets of measurements were taken during each run.

3.3 Sample Alignment

The reference mirror was always attached to the cryostat, and the other samples are aligned to match it. The complete alignment process is outlined in this section, including the reference mirror alignment which was not necessary for every experimental run.

The cryostat with the reference was placed into the sample chamber with the o-ring in place to allow the cryostat to be mounted in the correct position more easily during the alignment. Using the tungsten light source or the alignment laser feature in the Bruker spectrometer, the incident mirror was adjusted using the two alignment screws on top of the mirror so that the incident beam was centered on the reference. A piece of paper was placed in front of the collection mirror to show the position of the reflected spot. If the spot was not centered on the collection mirror then the required adjustment was estimated visually. The cryostat was removed from the sample chamber, trial adjustments were made to

the alignment and the cryostat was placed back in the sample chamber to re-check the alignment. This process was repeated until the reflected spot from the reference was centered on the collection mirror. Most often, the reference holder could be attached to the cryostat, and with the two main anchor screws evenly tightened the reference was properly aligned. If there was difficulty in aligning the reference then the cold finger on the cryostat could be rotated to adjust the horizontal (as viewed on the collection mirror) alignment, although this is not recommended for difficult sample alignments since all of the other cones would have to be adjusted to compensate.

When the reference was aligned, the other sample holders were attached and the cryostat was then placed in a support that held it horizontal for the next part of the alignment process. The support was designed to slide along a track allowing for easy transitions between samples during alignment. A laser held in a clamp on an optical post was adjusted to the level of the samples and clamped so that it was held active for the duration of the alignment. The laser projected a beam onto the row of samples that reflected the light onto a screen. The reflection from the reference was traced onto the screen using a pencil and the support was moved on the track so that the first sample was in the path of the laser. The orientation of the sample was adjusted so that the reflected sample spot was close to or on the center of the trace from the reference. It was useful to trace the sample spot (which was much smaller than the reference spot) once the alignment was finished so that the other samples could be aligned to it and the reference,

preventing the reflected spots from changing position between samples. This “external” alignment was repeated for the other samples. The cryostat was again placed into the sample chamber to verify that the reflected beams from all of the samples were centered on the collection mirror. The stage position was adjusted to move between samples in order to perform this check.

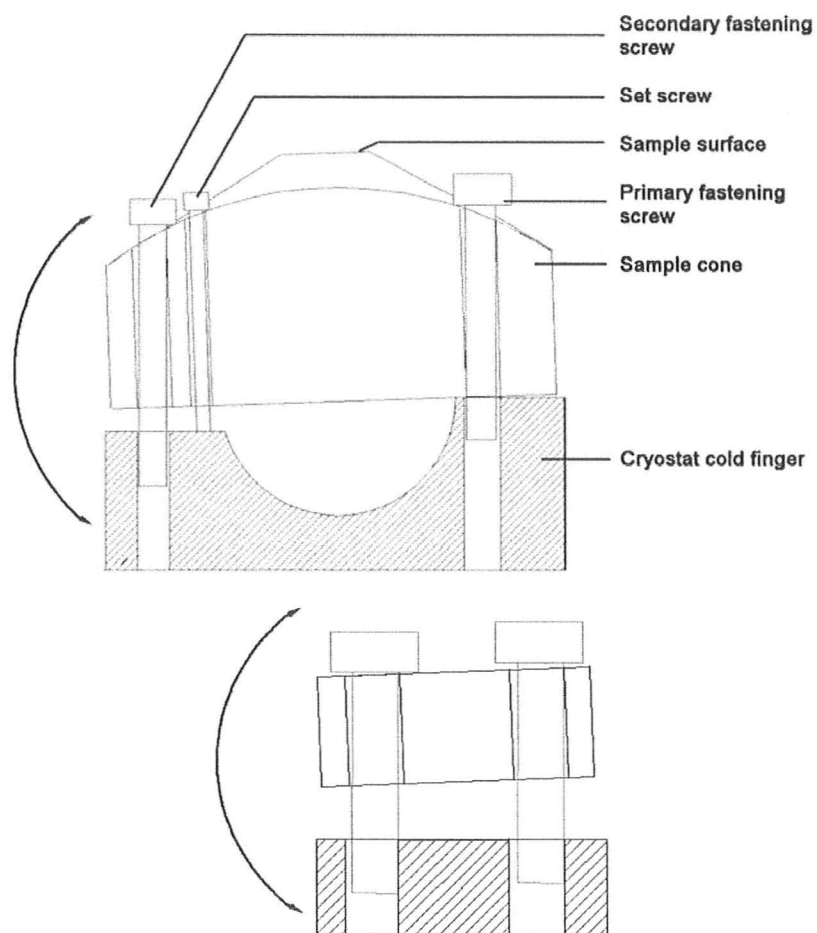


Figure 8 Illustration of sample holder and alignment.

Upper: a side view of cross section of a sample holder cone. Adjusting the screws as shows moves the sample image left or right on the collection mirror. Lower: cross-section view of the secondary fastening screw. Adjusting the screws as shown moves the sample image up or down on the collection mirror.

The final stage of the alignment was to ensure that the beam would be focused onto the detector. A piece of waxed paper with crosshairs drawn with pen on it was taped to the output port of the spectrometer and the alignment screws on the top of the collection mirror were adjusted to center the beam onto the output port. If the Mercury-Cadmium-Telluride (MCT) or photomultiplier tube (PMT) detectors were used they were attached to the output port of the spectrometer and the alignment and signals from each sample was checked before sealing the sample chamber. Using the MCT to check the alignment for the bolometers is not a reliable technique since the detector elements are different sizes, and the optimal alignment for different detectors may not always match. (Caution should be taken when adjusting the sample alignment screws to ensure that the amount of strain on the screws and holders is not too large. The soft brass of the holders gives way if the screws are too tight, resulting in damage to the sample cone, but no effective change in sample orientation. The screws may also break in extreme cases, leaving the remains threaded into the sample cone so that the cone must be removed in order to replace them and the alignment must be repeated).

3.4 Sample Cooling

The sample cones were mounted on the cryostat cold finger, which was made from copper, and connected to an R.G. Hansen and Associates HIGH-

TRAN cryostat. The cold finger shown in Figure 8 had a circular top to maximize contact with the base of the cryostat.



Figure 9 Cryostat cold finger with three samples mounted

Three samples shown here were mounted on brass cones, attached to the cold finger of the cryostat. The thermometer and heater wires for the cryostat were wrapped around the bayonet of the cryostat to reduce heat conducted from the room temperature connector for the temperature controller.

There was one platinum resistor (30 - 800 K) positioned close to the junction between the cryostat and cold finger as a “control” and a silicon diode (1.4 - 475 K) positioned on the sample rod behind the sample cones, between

sample positions 2 and 3 (numbered top to bottom). Both devices had 4-wire connections to reduce errors induced by resistance in the connecting wires. An electrical heater at the base of the cryostat was used to help stabilize temperature. All electrical connections for the thermometers and sample heater were made using a vacuum tight feed through that was connected to an external Lakeshore 330 Autotuning Temperature Controller. Thin constantan wires were used wherever possible and coiled around the cryostat bayonet to reduce conduction of heat from the room temperature surroundings through to the thermometers. An aluminum shield extension was also attached to the cryostat to absorb thermal radiation from the walls of the sample chamber. The aluminum shield was a cylinder with one closed end that was threaded at the top to screw on to the cryostat. It had four holes, 6 mm in diameter, for the light beam to reach the samples and one hole in the bottom for a limit switch.

Cooling was achieved using liquid helium-4 transferred through a flexible transfer line into the cryostat. The helium flow was controlled using a manually adjustable flow meter and aperture. The lowest temperature observed in this system was ~ 6 K; the lowest stable temperature achieved was 9.5 K, well below the transition temperature of interest for the HO phase. The complete spectrometer system, including helium Dewar and transfer line, is shown in Figure 10.



Figure 10 Complete spectrometer system with helium Dewar and transfer line.

The helium Dewar used for sample cooling is shown here, connected to the cryostat. The cryostat is fastened to the new translating stage and sample chamber. The 1 K bolometer was connected to the spectrometer.

3.5 Sample Chamber and Motorized Translating Stage

The cryostat with attached sample holders and shield were inserted into the sample chamber. The sample chamber was external to the spectrometer, made up of the cryostat, McAllister BLT4500 stage (See Figure 11), sample box, evaporator box and limit switch plate. The cryostat was inserted into the sample chamber, and sealed in place using a reusable Viton o-ring and a six bolt flange that connected to the top flange on the translating stage. The stage had a stainless

steel bellows between its base and translating stage that surrounded the cryostat to maintain the vacuum as the stage moved. The base was sealed to the sample chamber with a semi-permanent copper o-ring that was pressed between two six-bolt flanges. The sample box had two windows, one (polypropylene or KBr) on the sample port of the spectrometer, which was chosen using Table 1, and one quartz window opposite the first, for observing the evaporation process; both were sealed with Viton o-rings. The evaporator box was sealed to the sample box using a Viton o-ring. It also had an evaporator plate attached to one side, and a limit switch plate attached to the bottom. The sample chamber assembly is shown in Figure 12.

The translating stage had three “jacking” screws that rotated simultaneously using a gear and chain system connected to an Intelligent Motion Systems MDrive 23 stepper motor. The motor was connected to the computer used to operate the spectrometer and was controlled using LabView based software programs. The motor steps to vertical translation was 40,000:1.0 mm with accuracy of 5,000 steps, or 0.1 mm, where the uncertainty in position 5,000 the smallest step count that was used to optimize the sample position. The number of steps to optimize the sample position was chosen based on the number of steps required to remove backlash from the stage system (5000 steps). The stage itself had a flange that sealed to the cryostat with a Viton o-ring. A soft, reusable o-ring was chosen over a copper one because the cryostat was removed and re-installed

several times during an experiment to align the samples and remove the metallic coating at the end of each run.

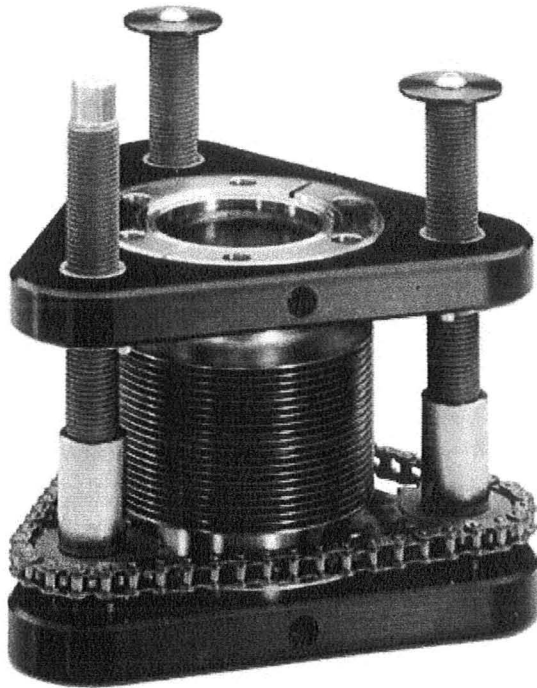


Figure 11 McAllister stage showing jacking screws and gear system, and bellows

The stage was moved using rotating screws, controlled by a gear system connected to an MDrive stepper motor. A stainless steel bellows was provided for vacuum capability.

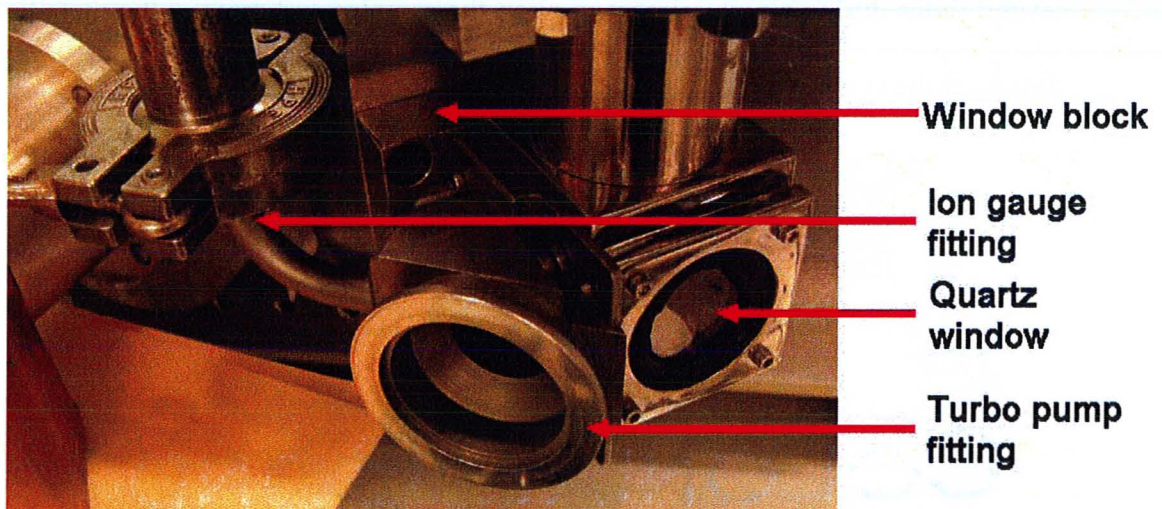


Figure 12 Sample box.

Shown with quartz window, turbo pump and ion gauge fittings, the window block that sat between the sample box and spectrometer output port is also visible

The sample box was a stainless steel tube with a cube at its base, with each face of the cube having a circular opening, with an o-ring groove and four 2-56 gauge holes for screws to hold a stainless steel plate in place to seal the chamber. As shown in Figure 12, the sample chamber was attached to a window block (Figure 13) that held either a polypropylene or KBr window. The exchangeable window block that was used for any given experiment was chosen according to Table 1, and depended on the spectral region of interest for that experiment. The window block isolated the sample chamber from the spectrometer chamber allowing for a better vacuum in the sample chamber and for separate ventilation of the optics chamber, if necessary, for final alignment procedures before a run, or for diagnostic work if a signal could not be obtained. The window was secured to the sample chamber using four 2-56 gauge screws

and was also secured to the spectrometer using four 4-40 gauge screws, both seams were sealed with Viton o-rings.

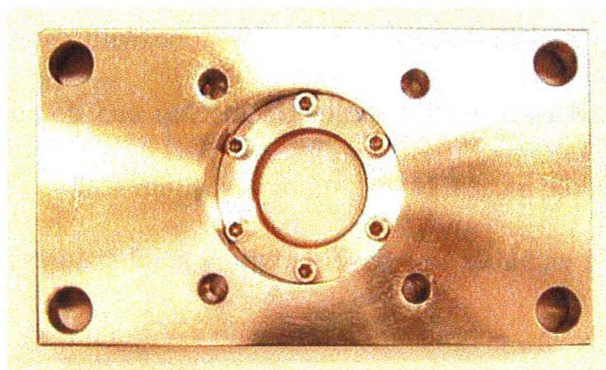


Figure 13 Window block

The window block was constructed of stainless steel, shown here with polypropylene window. Four small bolt holes around the window were used to attach the window to the sample box using 2-56 gauge screws. The four bolt holes at the outside corners of the window allowed for it to be bolted to the spectrometer using 5/16 – 24 gauge screws.

The sample chamber was evacuated using a Varian Turbo V-70 turbo pump that was connected to the side of the sample box. A special flange was attached to the left side of the sample box, sealed with a Viton o-ring. The flange had a QF40 fitting that matched the intake of the turbo pump, and an L-shaped tube with a QF25 fitting on the end where the bulb for an ion gauge could be placed to measure the vacuum in the system. The close proximity of the pump and gauge allowed for better vacuum and more accurate measurement of the vacuum than having the pump and gauge located several feet apart.

The face of the sample chamber that was most visible from the work station had a quartz window that was used to observe the glow from the

evaporation, and the movement of the sample holder as it moved with the stage. The window was held in place by a stainless steel plate with four 2-56 gauge screws and was sealed with a Viton o-ring that was a smaller diameter than the quartz window disc. Removing and replacing the window was done with care, since dropping or hitting the window could cause the edges to chip and could result in an uneven surface that would be incapable of forming a vacuum seal.

The fourth side of the sample chamber was covered with a solid stainless steel plate held in place by four 2-56 gauge screws and sealed with a Viton o-ring.

The combination of the bellows on the translating stage, the sample box, the evaporator box and the limit switch made up the sample chamber assembly. The parts of the assembly were aligned to make an irregular tube for the sample holder to fit into and move up and down in. The diameter of the tube in the sample chamber was 3.56 cm, and the diameter of the sample holder was 3.18 cm. The small amount of clearance made it important for the cryostat and sample holder to be centered carefully in the sample chamber assembly. This step followed the sample alignment and thermal shield attachment. The cryostat was inserted into the sample chamber assembly with the evaporator box removed. The Viton o-ring was placed between the cryostat and stage to ensure that the cryostat and sample holders were in the same position as they would be during the run. The stage was moved to a position that allowed the bottom of the sample holder to extend a short distance from the bottom of the sample chamber. As the nuts and bolts that hold the cryostat to the stage were tightened, the position of the sample

holder relative to the edges of the sample box was observed using a mirror. Later on, once the evaporator box and limit switch were in place, the centering was tested by moving the stage up and down in large steps to see if it would touch the sides of the chamber at any point. If the sample holder touched the side of the sample chamber, the nuts on the cryostat were adjusted and the motion of the stage was tested again.

3.6 Evaporation Chamber

The evaporator box shown in Figure 14 was used to hold three evaporator filaments and directed the vaporized coating material toward the samples when the stage was in position. The evaporator box was placed underneath the sample box to avoid having to move up a larger distance to clear the spectrometer. The evaporator box had a hole bored through it to form a tube to allow the sample holder to sit inside the box. The box also had a perpendicular hole that met this sample tube to form a T-shaped chamber so that the vaporized material from the filaments was ejected inward, toward the vertically aligned samples. Having a tube for the evaporation instead of the open face of a box prevented the vaporized material from travelling far into the sample chamber and helped to direct it at the samples. The evaporator plate was situated between the sample chamber assembly and the spectrometer so that no rotation of the sample holder would be required to perform this evaporation. The limit switch located at the bottom of the evaporator

box was used as an indicator for the correct evaporation position, and served as a reference point for the absolute position of the sample stage; the limit switch and light path were 9.4 cm apart. All seams on the evaporator box (between it and the sample chamber, limit switch plate and evaporator plate) were sealed using Viton o-rings.

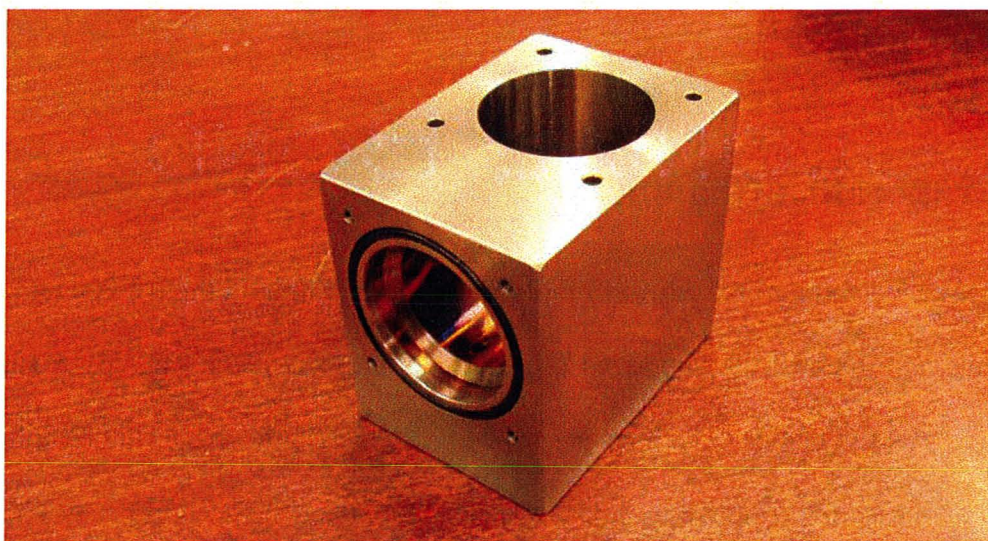


Figure 14 Evaporator box.

The evaporator box is shown oriented as it would be on the sample chamber assembly: the tube for the sample holder sits vertically, with the hole for the evaporator plate oriented perpendicular to the sample tube. When the evaporator plate and sample holder are in place, both are vertical and aligned for the vapour released from each filament to be directed onto the samples.

The evaporator plate held three filaments for evaporation onto the three samples and was removable for easy replacement of used filaments. The filaments were arranged vertically with two electrical feedthroughs for each filament, made from 2-56 gauge threaded stainless steel, as shown in Figure 15. The rods were

electrically isolated from the stainless steel plate by MS907 epoxy. The feedthroughs extended out of the back of the evaporator plate far enough for electrical leads to be connected to them, but not so far that they touched the spectrometer (approximately 4 mm.) The electrical leads were made from plastic insulated electrical wires with female banana plug sockets on the ends. During the evaporation, electrical current was applied to the leads, heating the filament so that the gold (or aluminum) was melted and then vaporized in the evaporation chamber (8 A for gold, 9 A for aluminum). The filaments were fastened to the threaded rods using a set of two nuts and two washers – the first nut adjusted the height of the filament above the plate, the filament was sandwiched between the two washers and the second nut was tightened to squeeze the washers together onto the end of the filament. Before each run the evaporator filaments were removed, and the plate was cleaned with acetone ensuring that no gold film would short the insulated leads. The evaporator box was similarly cleaned.

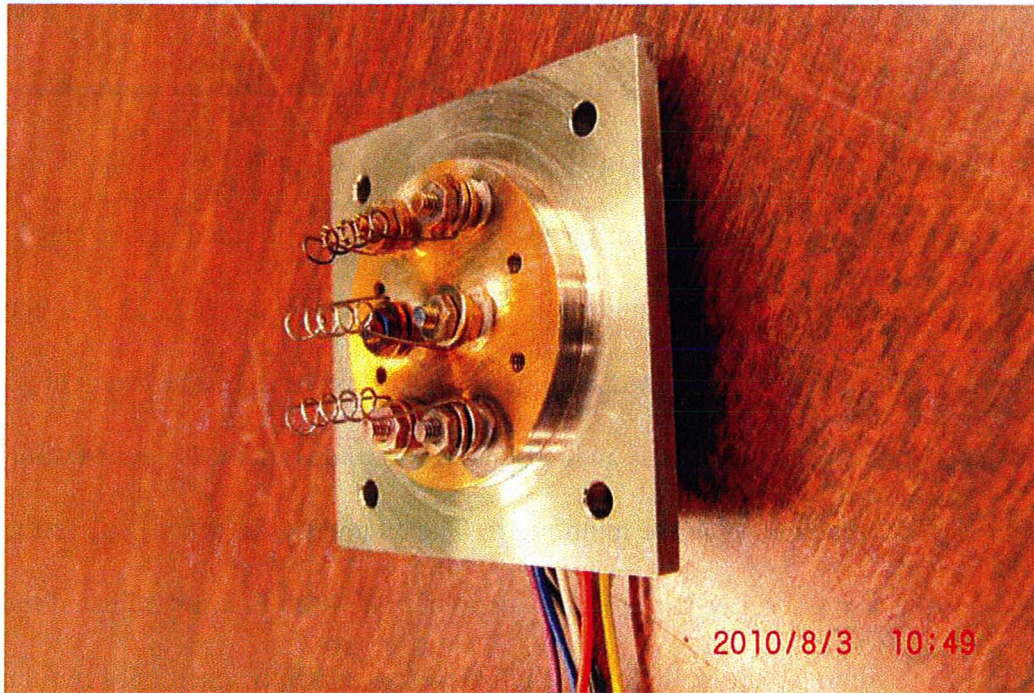


Figure 15 Evaporator plate with filaments and leads attached

The plate is shown after an evaporator test where the bottom two coils were fired and the top one was not. The top filament is discoloured from the gold evaporated by the other filaments.

The filaments were made using 0.04 cm diameter tungsten wire that was cleaned by holding one end in a vice, and sanding a length of it with fine sandpaper before wiping with a Kimwipe and acetone. The wire was then coiled ten or eleven times around a 2 mm hex-key held in a vice. The filaments were made and cut to have arms of about 3cm for them to be mounted onto the plate. The arms of the filament were held in a tabletop vice and three 7 mm long pieces of wire made from the desired coating material were cut and wrapped around the coils of the filament. The filament was removed from the vice and the arms were bent 90° so that the coil would sit evenly across its leads. The nuts and washers

were attached to the evaporator leads and one at a time, the bent arms of the filament were placed between the two washers and the nuts were tightened to secure it. The filament was then washed with acetone using a Kimwipe folded to form a corner. This process was repeated for the other two coils. The electrical wires were connected to the back of the plate and a multimeter was used to check the resistance across the filaments and between the filaments and the plate to make sure that it was not grounded. The plate was then attached to the evaporator box, ensuring that the Viton o-ring was in place and the four fastening screws were tightened. A second electrical check was done to make sure that the filaments weren't touching the walls of the evaporation chamber. The final stage of fitting together the sample chamber assembly was to attach the evaporator chamber and limit switch plate to the sample chamber. The bottom of the sample chamber was attached to the evaporator box and limit switch plate. Four 2-56 gauge brass rods were screwed into the bottom of the sample chamber and pass through clearance holes in the evaporator box and the limit switch plate. A nut was tightened on each rod to secure the assembly together. The rods needed to be removed in every run in order for the evaporator box to be cleaned and reset with new filaments for evaporation. The rods were brass so that if they got stuck in the sample chamber they could be removed more easily than if they were stainless steel. Since they were a soft material, care was taken not to tighten the nuts so much that they stripped the threads on the rods.

Once the assembly was complete the stage was moved up and down to ensure that it did not drag against the edges of the chamber and to check that the limit switch worked. The chamber was pumped overnight using a turbo pump to $\sim 3E-5$ Torr or better, which is required for a high quality coating on the samples, and reduces the amount of water vapour or ice that can contaminate the reflectance measurements (Homes *et al.*, 1993). Figure 14 shows the complete sample chamber assembly.

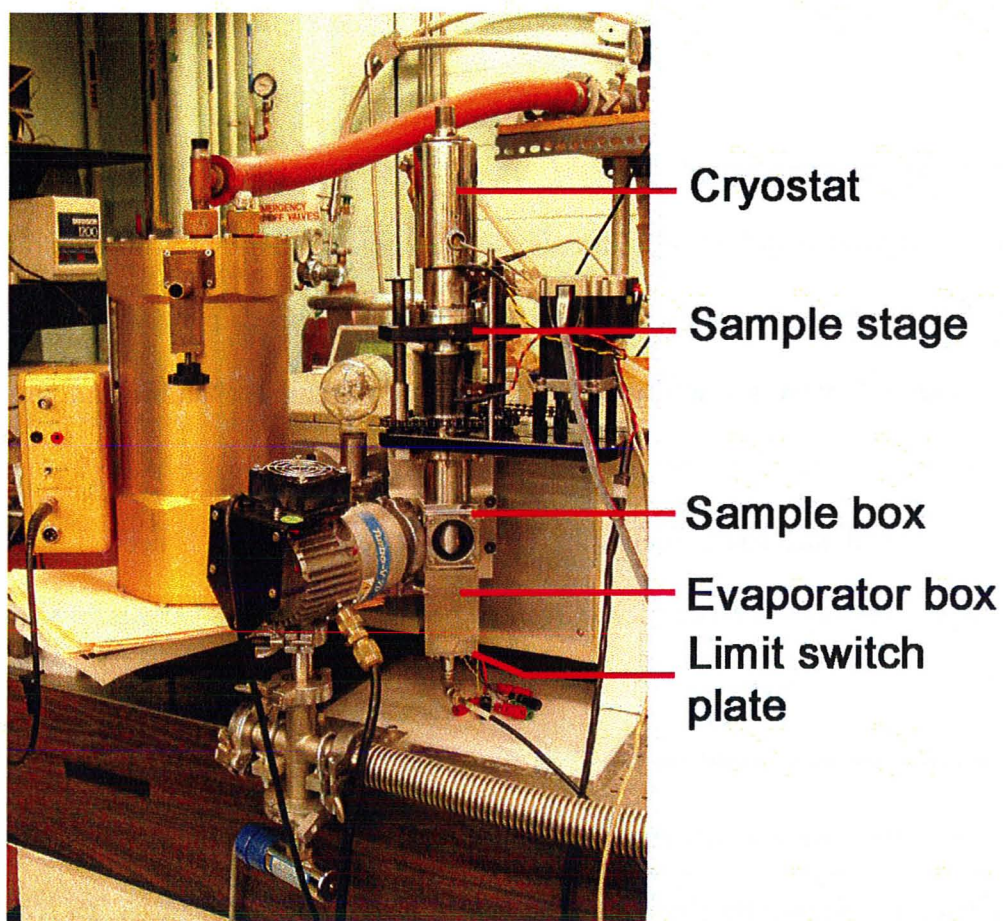


Figure 16 Complete sample chamber assembly

The external sample chamber is shown here, with external 1 K bolometer on the left side.

3.7 Detector Preparation and Acquiring a Signal

For the measurement of samples in the different spectral ranges required, a number of different detectors were used. The different detectors required different methods in preparation of the detector, and in acquiring and optimizing the signal. These procedures are outlined in this section. The two lowest frequency ranges that were measured are the FIR regions which were measured using the 1 K and 4 K bolometers. The MIR and NIR regions were measured using a Mercury-Cadmium-Telluride (MCT) detector and the VIS-UV region was measured using a Photomultiplier Tube (PMT). The procedures for preparing these detectors up to acquiring a signal are outlined in the following sections.

3.7.1 1 K and 4 K Bolometers

The preparation of the two bolometers was very similar: they were pre-cooled with liquid nitrogen, and then filled with liquid helium. In the case of the 1 K bolometer the helium chamber was evacuated using a mechanical pump to bring the temperature of the bolometer element to 1.8 K. The bolometers were produced by Infrared Labs (models LN-6B for the 1 K bolometer and LN-6C for

the 4 K bolometer) and were made up of four main components: the silicon bolometer element, a 3 L helium Dewar, a nitrogen Dewar with attached thermal shield, all inside of an evacuated jacket chamber. The 1 K bolometer was used to measure 20 - 250 cm^{-1} and had a holding time of ~ 26 h, while the 4 K bolometer could be used to measure 25 - 600 cm^{-1} and lasted ~ 40 h.

The day before a run was scheduled, the bolometer jacket was pumped using the diffusion pump to $2\text{E}-6$ Torr or better. The bolometer was placed on a stool next to the diffusion pump and a rubber hose with a QF16 connector fitting on one end was used to connect the bolometer vacuum valve to the pump. Before turning on the roughing pump, the backing valve was verified to be closed. The roughing pump, fan and diffusion pump were turned on in sequence, and the nitrogen tank for the diffusion pump (used to cool the walls of the oil chamber in the pump so that the oil vapour condenses and is recovered) was filled while the pump warmed up. The roughing valve was opened first, to clear the vacuum lines between the pump and the jacket. When the pressure approached 60 mTorr the jacket valve was opened slowly. Opening this valve too quickly could result in loosening of the aluminum foil thermal shielding that surrounded the helium and nitrogen tanks causing the shielding to become a thermal ground if it touched the jacket and the helium tank; this would significantly reduce the holding time of the bolometer. When the jacket pressure reached 60 mTorr the roughing valve was closed and the backing valve was opened, the diffusion pump chamber was operated for a few moments until the pressure reached <50 mTorr. (The roughing

valve and backing valves should never be open at the same time, this leads to air being introduced to the hot oil chamber that is the mechanism of the diffusion pump causing the oil to burn and the pump could be permanently damaged). Once the pressure gauge on the diffusion pump and vacuum line read $<50\text{mTorr}$, the baffle valve for the diffusion pump was opened. The pump was left on overnight, filling the nitrogen tank every ~ 10 hours until the jacket pressure was $2\text{E-}6$ Torr or better.

Once the jacket pressure was suitably low, the jacket valve and baffle valve were closed. The bolometer was removed from the diffusion pump system, the diffusion pump was turned off, but the fan and roughing pump were left on while it cooled, the backing valve was also left open for the roughing pump to pump on the hot oil chamber of the diffusion pump.

Before beginning the helium transfer the helium transfer nozzle was attached to the helium tank of the bolometer (The nozzle had a compression fitting in the top and a nozzle that tapered at the end to ~ 1.27 cm dia.) The depth of the helium tank in the bolometer was measured and marked on the short end of the helium transfer line, the bottom and liquid levels in the helium Dewar to be used for the transfer were measured and marked on the long end of the transfer line. Books and a wooden support were used to raise the bolometer to a height where the transfer line would be level and reach the bottom of the bolometer tank and the liquid in the Dewar simultaneously.

The helium tank was pre-cooled using liquid nitrogen to reduce the amount of helium required for the transfer. There were two L-shaped transfer lines with latex hoses attached for this purpose, one long and one shorter. The long one was for the helium chamber which was the central opening in the lid of the bolometer. The tube fit into the Dewar so that the compression fitting on the top of the tank made a seal with it. The latex tube was connected to the nitrogen Dewar and the nitrogen valve was opened. Liquid nitrogen flowed through the transfer line into the helium chamber and any boiloff escaped from the nozzle in the top of the tank. When liquid nitrogen came out of the nozzle, or when the exhaust had a flame-like appearance the transfer was stopped, it usually took less than 20 minutes depending on the pressure in the nitrogen Dewar. When liquid nitrogen began collecting in the tank, a multimeter connected to the thermometer output of the bolometer read $\sim 140\Omega$. A heat gun was used to soften the latex hose so that it could be removed from the nitrogen Dewar and the hose from the L-shaped transfer tube in the nitrogen tank was connected to the nitrogen Dewar. The nitrogen tank in the bolometer was filled until liquid boiled out of the top. The transfer line was not sealed in this case and the nitrogen that boiled off escaped through the top of the nitrogen tank. Once the nitrogen tank in the bolometer was filled, the end of the transfer line from the helium tank was placed inside a Styrofoam container, and dry helium was blown through the nozzle to purge the liquid nitrogen out through the transfer line. When the flow of liquid stopped, the dry helium gas line was removed and the return line for helium

recovery was attached to the nozzle. The return line was a small length of rubber hose with a QF25 fitting on the end to connect to the metal pipes that were used to recover used helium during the transfer. Plastic hose was not used to return the helium; it freezes and breaks, and is also difficult to remove from the nozzle while frozen.

When the pre-cool was finished, the helium transfer was begun by moving the helium Dewar close to the bolometer so that the solid transfer line would not be bent for the transfer. The long end of the transfer line was inserted into the Dewar and lowered slowly to the mark for the liquid depth in the Dewar. The nitrogen transfer line was removed from the helium tank in the bolometer and replaced with the helium transfer line. The switch was be done quickly to avoid getting any air or water vapour into the helium tank, the dangers being that the helium would liquefy the oxygen from the air, and the formation of ice in the tank. The transfer line was lowered into the bolometer tank and the Dewar until it reached the bottom of the bolometer tank and was below the liquid level in the Dewar. Books were used to change the height of the bolometer to make sure that the transfer line was not bent. The relevant valves on the return system were opened and the volume meter reading on the helium recovery line was recorded. The transfer took 20 minutes or 5 L of liquid helium. When the recovery meter reading increased by 133 cu. ft. the transfer had returned 5L (plus 3 L in the Dewar). During the transfer, the batteries for the bolometer were replaced with fresh batteries for each run (both required 9V). A heat gun was used to keep the

top compression fitting on the bolometer from building up ice, it was prevented from freezing so that the o-rings inside it would not freeze and break. Towards the end of the transfer, or at the 20 minute mark, the return line was removed from the bolometer nozzle by opening it at the QF16 flange at the end of the rubber piece. This was close enough to the nozzle that the flame-like plume that indicates a complete transfer was not always observed. The thermometer resistance was checked and was typically 880Ω when liquid began to collect in the tank.

When the transfer was complete, the pressure in the helium Dewar was released and the transfer line was removed from the Dewar and bolometer tank. A plug was fit into the compression fitting of the bolometer tank to prevent air getting into it. For the 4 K bolometer this was the end of preparation. The rubber hose used for helium return was removed and replaced with a long piece of latex hose for helium exhaust while preventing air from coming up the hose into the tank. The bolometer tank was not connected to the return system because the return system is kept at a slight vacuum to facilitate recovery and this would increase the boiloff rate for the detector reducing its holding time. The bolometer was moved to the spectrometer where books were used to support it to the appropriate level and it was fastened to the spectrometer flange using two 4-40 gauge screws and sealed with an o-ring to allow the spectrometer chamber to be evacuated.

The preparation of the 1 K bolometer required that the nozzle used for the transfer be switched for another that had different vacuum pipe attached (see both

nozzles in Figure 15). It was sometimes necessary to heat the nozzle used for transfer with a heat gun so that it could be removed and replaced. The switch was done quickly to avoid letting air into the helium tank. With the vacuum nozzle for the helium tank attached, the bolometer was moved to the spectrometer and attached using two 4-40 gauge screws and sealed with a Viton o-ring. The vacuum nozzle in the bolometer helium tank was connected by a rubber hose to a mechanical pump, with gauge to monitor vacuum. The pump was turned on and the valve was opened very slowly (1/4 turn every minute) until the helium tank reached, then the valve was opened completely. Pumping on the helium tank reduced the temperature of the liquid helium to 1.8 K, which was indicated by a thermometer resistance of 9.4 k Ω .

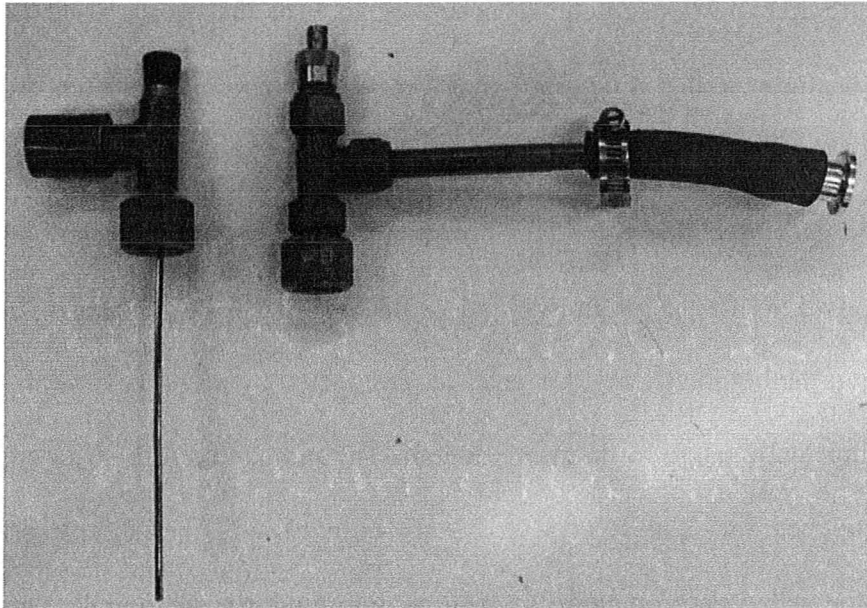


Figure 17 Bolometer nozzles for liquid helium transfer and vacuum pump

(Left) The vacuum nozzle with 2.5 cm diameter pipe that extended horizontally when screwed onto the top to the helium tank of the bolometer. It was connected to a mechanical pump using a rubber hose. In the top of the nozzle is a stopper in the tube that extended down the pip in the bolometer to the helium tank. If the vacuum nozzle became obstructed, build in pressure would eject the stopper and be released, preventing damage to the bolometer.

(Right) The transfer nozzle could also be screwed onto the top of the helium tank of the bolometer. The 1.5 cm diameter exhaust tube is shown here with the rubber attachment used to connect the exhaust to the helium return system. The stainless steel compression fitting and plug are seen attached to the top of the nozzle.

The nitrogen tank in the bolometer was kept filled for the duration of the experiment. This nitrogen cooled a thermal shield inside the bolometer jacket and helped to increase the holding time of the bolometer.

The bolometer was connected to a Stanford Research Systems SR560 Low Noise Pre-amplifier that was used to filter and amplify the signal before sending the signal to the spectrometer. The spectrometer signal was directed into the

computer where it was interpreted by a control program that displayed the interferogram or spectrum. The filter settings for both bolometers were 0.03 low pass, 1k high pass and 1000x gain. Once a signal was acquired by the computer, the final step of alignment was done before evacuating the spectrometer. The alignment knobs of the incident and collection mirrors were adjusted one at a time to maximize the signal obtained from the reference mirror. The auto align function of the spectrometer was not used in the FIR experiments since this region has longer wavelengths, it would require large movement of the mirrors and aside from taking a long time, was found to be ineffective. Once the signal was optimized, the spectrometer chamber was evacuated. Since the mercury arc lamp was used in this spectral region it was turned on before the spectrometer was evacuated, and required 1 - 2 hours to stabilize before measurements could be made. For this reason, bolometer preparation was done in the evening before a run.

3.7.2 Mercury-Cadmium-Telluride (MCT) Detector

The MCT detector operated at 77 K and was cooled using liquid nitrogen. The nitrogen container had a capacity of <1 L and was “topped up” frequently during the day, it had a holding time of 8 – 10 h. The MCT was fastened to the spectrometer with four 2-56 gauge screws and sealed with a Viton o-ring. The

signal output was connected to a primary preamplifier with a battery power supply of 12 V. The batteries used were automotive lead/acid batteries that have long lifetimes and no alternating current (AC) noise. The 10x gain of the primary preamplifier was connected to the input of the Stanford preamplifier (the same one used for the bolometers) with low pass, high pass and gain settings at 3, 30k and 2x respectively for measurements in the MIR region and 30k, 100k, 2x for the NIR region. The primary preamplifier was kept on a polyurethane foam base to reduce noise in the signal caused by vibration.

The procedure was similar to one used for the bolometers. The signal from one of the samples was optimized by adjusting the alignment knobs on the incident and collection mirrors in the spectrometer. If the NIR region was being measured, the tungsten light source was turned on before evacuating the spectrometer chamber. The MIR source – the globalar, was always left on. Once the spectrometer chamber was evacuated, the auto align feature of the spectrometer was used to further improve the signal from the sample.

3.7.3 Photomultiplier Tube (PMT)

The PMT was a room temperature detector, and needed only to be fastened to the spectrometer with two 4-40 screws and sealed with an o-ring. It was connected to a variable voltage DC power supply and the applied voltage was

increased until the output signal was between 0.2 and 0.3 volts (the PMT overloads at 0.5V). Each sample was sequentially moved into the light beam and the output voltage was observed to determine which sample provided the largest signal. The stage was moved to the reference position and the collection mirror was adjusted to optimize the signal strength output by the detector. The stage was then moved to the sample with the strongest signal (which was sometimes stronger than the reference signal) and the DC voltage was increased until the output signal was $\sim 0.4V$. The signal was optimized with care to avoid overloading the detector during the experiment. All of the optimization was performed with the laboratory lights out so that the ambient light from the lab would not overload the detector. The detector output was then connected to the preamplifier with low pass, high pass and gain of 300, 300k, 100x respectively.

3.7.4 Data Acquisition Software

The OPUS (version 3.1) software program supplied by Bruker was used for collecting and analysing data. OPUS was run on a Windows 97 desktop computer. This program was used for computer controlled selection of the light source being used, the aperture size, scan speed and resolution. Most of the features were controlled through the “Measurement” window presented by the software, and viewing the spectrum or interferogram being measured was as easy

as selecting the “check signal” tab in this window. If a signal did not appear, the settings in the program for light source, beam splitter and aperture size were checked. The file path for saving scans was also controlled in the measurement window. When first opening OPUS, the file path and operators were updated by selecting the measurement menu. In the acquisition tab, a measurement program was selected according to Table 2.

After selecting the correct measurement program the file path, file name and operator names were changed, and saved. The light source and beam splitter selections in the program were checked on the “Optics” tab and corrected if necessary. The changes were executed by clicking on the “Check Signal” tab. Once the correct file path and name were entered, and the correct components selected, measurements were collected at room temperature, low temperatures (12.5 K, 25 K, 50 K, and 100 K) and then room temperature again, followed by the evaporation and another temperature cycle to obtain the full set of spectra required to calculate the absolute reflectance of a sample.

4 Measurement Procedure

In the previous chapter the equipment and assembly of the spectrometer system were discussed. This chapter continues the discussion of the method of obtaining reflectance measurements from 12.5 - 300 K in the FIR, MIR and NIR spectral regions and at 300 K in the VIS/UV region. Since the temperature dependence for the samples was not the same for each spectral region, different temperatures were measured for each spectral range, as shown in Table 3. These procedures were begun after the sample chamber had been assembled and pumped overnight to $\sim 3\text{E-}5$ Torr or better, and after the detector had been attached and final signal optimization had been performed. The spectrometer configuration of beam splitter, sample window, detector, etc. was chosen using Tables 1 and 2. Measurements were run at room temperature to first establish a baseline or reference point for the spectra; measuring the samples at room temperature at various times during the run (see Section 4.1) helped to provide data for diagnostics used to determine the stability and accuracy of the measurements made during that run. The sample holder was then cooled to its lowest temperature using a liquid helium flow cryostat. At the lowest temperature the flow of helium was reduced to allow the temperature to rise and stabilize at 12 K to within 0.5 K. It was not always possible to stabilise the temperature at 12 K due

to the pressure in the liquid helium Dewar, and so for the 4 K bolometer measurements 13 K was the lowest possible temperature.

Frequency Range	Sample Temperatures (K)
25 - 235 cm^{-1} (FIR)	12.5, 25, 50, 100, 150, 200, 300
35 - 600 cm^{-1} (FIR)	13, 25, 50, 100, 150, 200, 300
400 - 6000 cm^{-1} (MIR)	12, 20, 50, 100, 150, 200, 300
3000 - 14000 cm^{-1} (NIR)	25, 50, 100, 150, 200, 300
13,000 - 38,000 cm^{-1} (VIS/UV)	300

Table 3 Temperature steps taken for each spectral range.

For the URu_2Si_2 sample and the other samples being measured in the same experiments, the critical temperatures were close to 20 K. The URu_2Si_2 sample had no temperature dependence above 450 cm^{-1} (Bonn *et al.*, 1988) and so small differences in temperature would not affect the absolute reflectance when the measurements were merged together. For example a 14 K MIR spectrum could be merged with a 13 K FIR spectrum without any measureable effect since the MIR data was temperature independent. The 13 K and 12.5K FIR data sets were merged because of the small temperature difference between them.

In order to account for thermal contraction of the cryostat and cold finger during the experiment, the sample signals were each optimized by observing a real-time “Check signal” display in OPUS, and moving the sample stage up and down by steps of 0.25 to 0.125 mm in order to maximize the amplitude of the spectrum. The signals were optimized at room temperature, at the lowest temperature, and if the difference between two temperature steps was 50 K or

larger. Between room temperature and the lowest stable temperature of the cryostat, the changes in sample positions were as large as 1 mm.

4.1 Measurement Procedure for the FIR, MIR and NIR Spectral Ranges.

At each temperature spectra were collected using OPUS. Each measurement consisted of 100 scans of the spectrometer that were averaged by OPUS and saved. The measurements at each temperature were repeated five times and averaged together – a total of 500 scans were averaged to produce one reflectance spectrum that was used for further calculations outlined in Chapter 5.

The measurements were separated into 100-scan segments for diagnostic purposes: if the first and last measurements did not agree within 0.5% it indicated a problem that needed to be diagnosed and corrected. Common problems included lamp instability or a change in sample position (forgetting to take out backlash, helium transfer line putting transverse pressure on the cryostat). One unique problem that was encountered was that as the cryostat jacket cooled as liquid helium flowed through it, the heater in place to keep the o-rings in the cryostat from freezing was heating the jacket unevenly cause uneven thermal expansion in the jacket that resulted in a change in the position of the cold finger and sample holders that were attached to the cryostat. A direct relationship was observed between a 1% change in signal amplitude and the on/off cycle of power to the jacket heater (controlled by a proportional controller with a platinum resistor used

as the thermometer). This problem was solved by replacing the platinum resistor, and changing the variable voltage output for the heater as the cryostat underwent large (~ 100 K) changes in temperature.

After a set of five measurements were recorded for a sample at temperature, T , the stage was moved to the position of the next sample that was determined using the optimization method outlined above (~ 1 cm), and another set of five measurements were made. In this manner measurements were recorded and averaged for all four samples. The reference signal was measured twice at each temperature step, either before and after measuring the samples (reference, sample 1, sample 2, sample 3) or even spaced between the sample measurements (sample 1, reference, sample 2, reference, sample 3). The purpose was to achieve higher accuracy in the reflectance calculations by reducing the amount of time between a sample and reference measurement that were to be used in the same absolute reflectance calculation. Having two reference measurements at the same temperature, spread out over time also provided an indication of the stability of the signal over the time taken to record the measurements for all of the samples at each temperature. Stability of $<0.5\%$ was considered acceptable, meaning that the signal being measured changed by $<0.5\%$ during the time taken for the spectrometer scans to be completed. This magnitude of systematic error when allowed to propagate through the data analysis will result in an error that is substantially larger, for example in the conductivity. Since the conductivity depends on the difference between the 100% line and the measured data the error

can get very large for reflectances close to 100%. For example, in the Drude model the absorption ($1 - R$) is proportional to $\sqrt{\rho}$, at a reflectance level of 95% a 0.5% error would result in a 20% conductivity error.

After completing measurements at one temperature step, the flow of helium was further reduced to allow the sample holder to warm up to a higher temperature. For temperatures above 18 K it was necessary to turn on the electrical heaters connected to the temperature PID controller. Depending on flow rate and Dewar pressure the heater strength could be adjusted to low, medium or high, and the PID controller adjusted the power of the heater to control the temperature to within 0.5 K. After measuring the samples at low temperatures, the cryostat was returned to room temperature and a second set of room temperature measurements were recorded and compared to the first set of room temperature measurements. It was not uncommon for the difference between the two room temperature sets of data to be 1 – 5%, but the difference could be explained by drift and the sum of small system changes (drift in lamp power over a long period of time, thermal expansion in the spectrometer system as the lamp warmed up) that may have occurred over the 7 – 9 hours that it took to measure the samples at all of the temperature steps involved. This error was corrected using measurements of the reference mirror as outlined in Chapter 5.

The second phase of the experiment was to measure the samples with a coating of known material in order to correct for surface irregularities. Gold was used for the FIR, MIR and NIR spectral regions and was measured between

temperatures of 15 – 300 K in similar temperature steps as the first phase. For the experiments outlined in this thesis the gold was not measured at exactly the same temperature steps, as is usually done, but the change in the gold spectrum between 10 K and 25 K was known to be minimal and the 15 K spectrum of the gold coated sample could be used in the absolute reflectance calculations for the sample at both 12.5 K and 25 K.

After the second set of room temperature measurements were completed, the sample stage was moved to the limit switch position where the samples were aligned with the evaporator filaments. Each evaporation filament was “fired” individually by connecting the external leads to a power supply and increasing the current slowly from 0 to 6 A to melt the gold and wet the tungsten filament, and then increasing the current to 8 A to vaporize the gold. A successful evaporation was marked by a slight, temporary increase in the pressure of the sample chamber during the vaporization of the gold, and a change in the resistance of the filaments after the evaporation. The reference mirror was excluded from the evaporation step since the evaporation chamber was designed to evaporate on the three samples and the reference was positioned outside of the cavity in the evaporator chamber where the filaments were held. Occasionally some gold got on the reference mirror, and this was corrected by switching to a gold reference mirror and by making a correction to the absolute reflectance calculation discussed in Chapter 5.

The coating on the samples was observed after the evaporation procedure by moving the stage back to the sample positions and measuring the spectra at room temperature a third time. These measurements were for similar diagnostics as the first and second room temperature measurements, and for corrections to the absolute reflectance if the spectrum of the reference mirror changed at all when compared to the spectrum before the evaporation. After the measurements at room temperature, reflectance measurements were taken at 15, 25, 50, 100, 150, 200 and 300 K on the coated samples using the same procedure described above: optimizing on the samples for large changes in temperature steps, and measuring all samples with reference twice as a stability check. The room temperature reference measurements from the beginning of the run and after the low temperature measurements on the coated samples at the end of the run were compared to check the stability of the whole run. These values were within 5 - 10%. This relatively large variation was attributed to the effects of the metal coating, the drift in the spectrometer and detector over 12 - 20 hours, and other factors that have yet to be identified and reduced.

4.2 Measurement Procedure for the VIS/UV Spectral Region

In the VIS/UV region there was no expected temperature dependence in the reflectance spectra for any of the samples, so low temperature measurements were not necessary. The spectra for each of the samples were measured at room

temperature, before coating the samples with aluminum, and measurements were then taken of the coated samples. The same procedure for evaporating the aluminum onto the samples was the same as for gold, except that the current was raised to 9 A to vaporize the aluminum. Aluminum was used instead of gold for the VIS/UV range since it has no absorption in this region and gold does.

5 Data Analysis

Chapter 4 described the method of obtaining reflectance measurements required for calculating the optical properties of a material, this chapter discusses the analysis and results of the measurements of URu_2Si_2 . The first section covers the thermal reflectance measured by Dr. Nagel and Dr. Rößm (2010) and an attempt at refining the absolute reflectance data obtained from those measurements. The second section discusses the analysis of the absolute reflectance from my measurements made at McMaster and the calculation of the optical conductivity from these absolute reflectance measurements is covered in Section 3. This section includes the extrapolation methods used to extend the data for Kramers-Kronig (KK) analysis.

5.1 Thermal Reflectance and Refinement of the Absolute Reflectance at Low Frequencies

Thermal reflectance ($t_T = R_T/R_{20}$) measurements can be used to examine a phase transition or energy gap by giving a direct comparison of the reflectance of a sample above and below the critical point of the transition. The advantage for this type of measurement is that the sample does not have to be moved between

measurements, and therefore is more accurate and free of fringes. The thermal reflectance of the URu₂Si₂ sample grown at McMaster was calculated from the data collected in my experiments, and compared to results from two collaborators, one in Tallinn, Estonia (Nagel, U., 2010) and the other in Paris, France (Lobo, R., 2010). The French data was shown in Figure 2 and seemed to have two smaller peaks associated with the gap of the hidden order transition. In order to further investigate the HO transition, reflectance measurements were made by our group, at McMaster University, at temperatures between 10 and 20 K (where 20 K was considered to be in the “normal” state) for a frequency range from 20 – 250 cm⁻¹. For thermal reflectance measurements it was not necessary to coat the samples with gold. The thermal reflectance at temperature T, t_T , was calculated by $t_T = R_T/R_{20}$ where R_T was the reflectance at T, and R_{20} was the reflectance at 20 K. The calculations for the data collected in Hamilton had to be normalized to 1 at 100 cm⁻¹ since the lamp was unstable for some of the earlier measurements and the beam splitter minima at 60 cm⁻¹, 130 – 140 cm⁻¹, and 200 cm⁻¹ made it difficult to determine the scaling factor. The thermal reflectance shows the same general behaviour as the French thermal reflectance in Figure 2 (Lobo, R., 2010): a minimum in reflectance at 36 cm⁻¹ that shrinks with increasing temperature, shown in Figure 14. At 10 K the depth of the minimum determined from the Hamilton experiment was 0.942 at 40 cm⁻¹, with a 0.4% difference compared to the French data from Figure 2, and a 0.2% difference compared the Estonian data, shown in Figure 15 (Nagel, U., 2010).

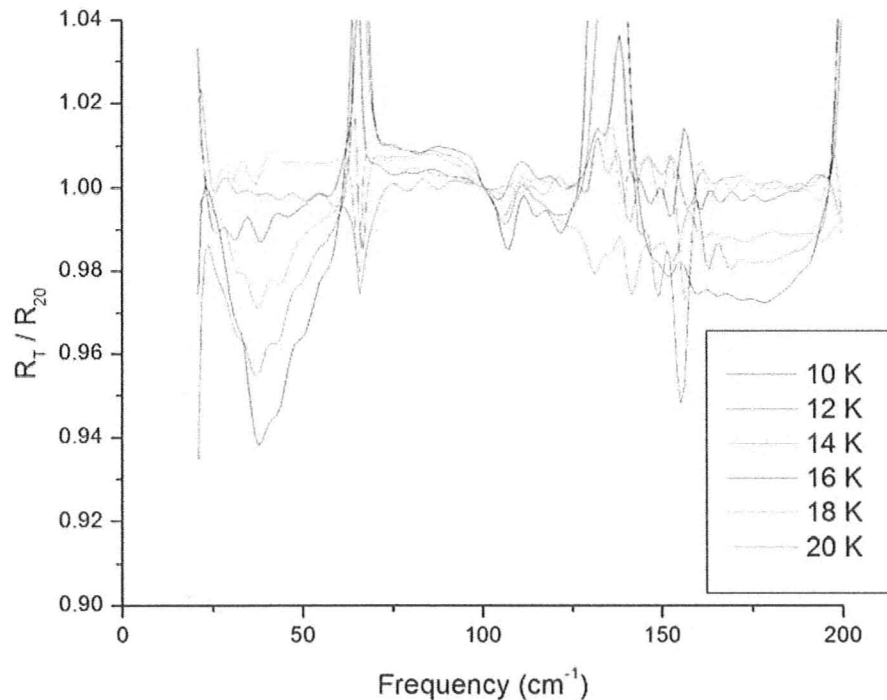


Figure 18 Thermal reflectance of URu_2Si_2 measured in Hamilton, Canada

The thermal reflectance shown here was normalized at 100 cm^{-1} , using the equipment and methods outlined in Chapters 3 and 4, with one exception: the sample was not coated with gold, simply measured repeatedly between low temperatures and the “normal” state temperature 20 K. The peaks at 60 cm^{-1} , $130 - 140\text{ cm}^{-1}$ and 200 cm^{-1} were caused by beam splitter minima in the $50\text{ }\mu\text{m}$ Mylar beam splitter used for the experiment. The HO related minimum in reflectance is at 40 cm^{-1} , and decreases in size as temperature approaches $T_0 = 17.5\text{ K}$.

As discussed in Chapter 2, the thermal reflectance can be used to determine gap size and symmetry. Since the thermal reflectance shown here is distorted by beam splitter minima, and the thermal reflectance recorded by Dr. Nagel in Figure 15 (2010) has no such effect, the interpretation of the thermal reflectance is left to those with better data.

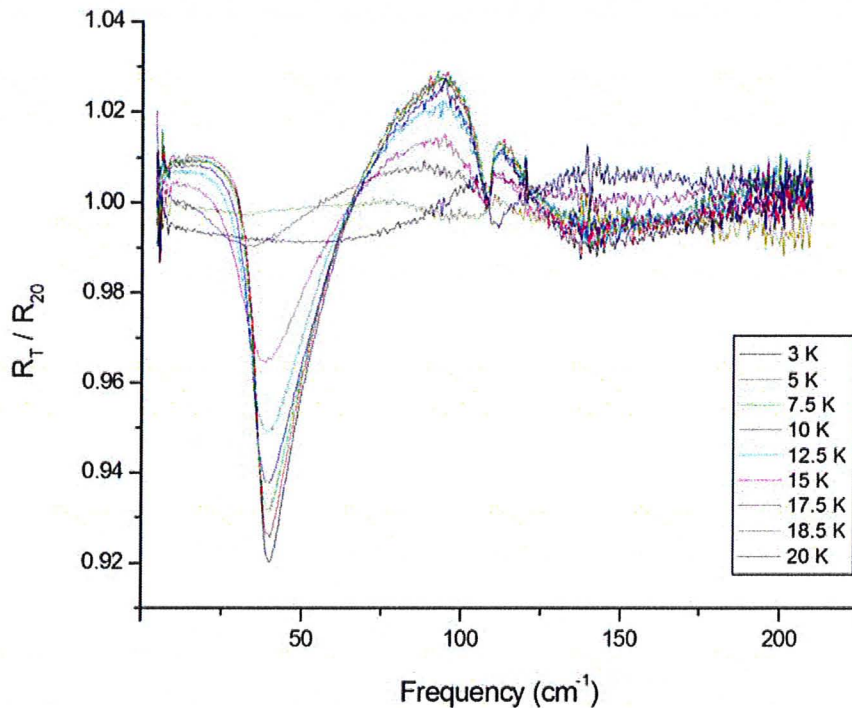


Figure 19 Thermal reflectance of URu_2Si_2 (Nagel, 2010).

The data provided by Nagel *et al.* shows the HO gap that opens at 17.5 K and deepens with decreasing frequency. Unlike the measurements made using our equipment, no beam splitter minima are present since a 100% efficient polarizing beam splitter was used in the Martin-Puplett type spectrometer used in these measurements.

The URu_2Si_2 sample that was measured in Tallinn, Estonia was grown at McMaster by the Luke group. The experiments were conducted using a Martin-Puplett spectrometer and 0.3 K bolometer. The sample and bolometer were placed in an immersion Dewar with liquid. The measurements were taken at temperatures between 3 and 20 K. An absolute reflectance measurement was also taken at 3 K.

In an attempt to explore a curve smoothing method, the 20 K absolute reflectance was calculated from the 3 K thermal reflectance ($t_3 * R_3 = 1/R_{20}$). A cursory look at the data suggests that a parabolic approximation would be a good start to describe the data. The 20 K absolute reflectance data was fit using a linear regression fit to a parabolic curve: $P = 1 - p \omega^2$. The optimized linear fit of R_{20} vs. ω^2 produced $P = 0.9872 - 8.115E-6 \omega^2$ with a regression coefficient of 0.8417, shown in Figure 20. In place of R_{20} this fitted function P was used to represent our best approximation to the absolute reflectance at 20 K. A possible drawback of this method is the fact that any sharp feature that persists between 20 K and lower temperature is washed out. The 3 K thermal reflectance, t_3 , measured by Dr. Nagel (2010) was multiplied by the P to get the refined absolute reflectance, shown in Figure 21. The final result of the refined absolute reflectance at 3 K is shown in Figure 22. The standard deviation of the absolute reflectance compared to the refined absolute reflectance was ± 0.011 .

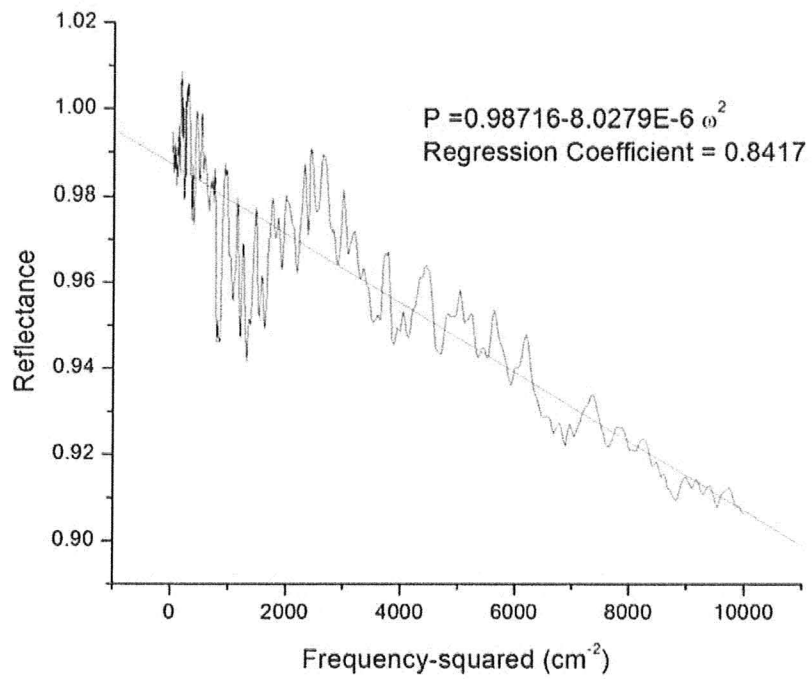


Figure 20 Absolute reflectance at 20 K (Nagel, 2010) plotted against frequency-squared for linear regression.

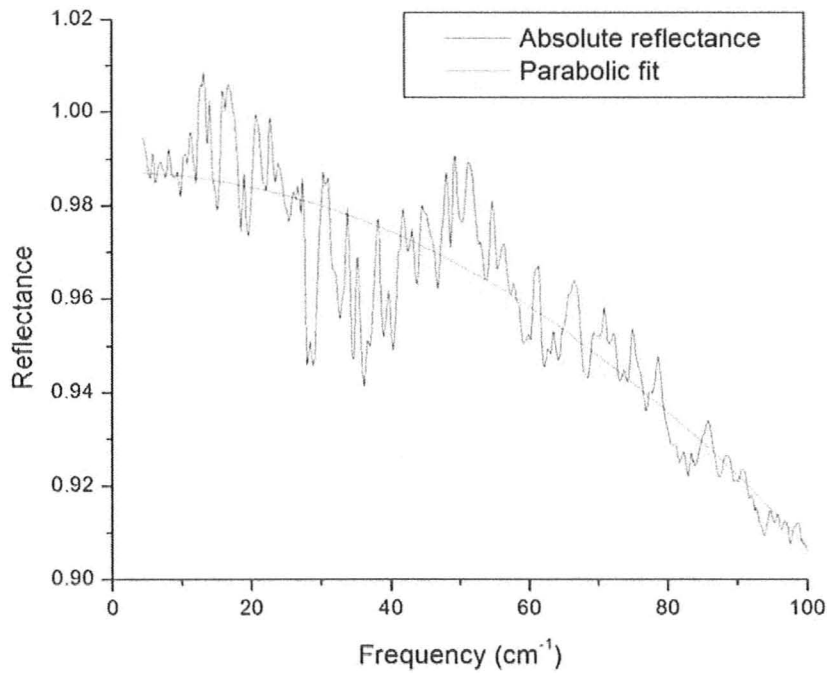


Figure 21 Parabolic fit to 20 K absolute reflectance from Tallinn (Nagel, U., 2010)

The black curve shows the absolute reflectance measured in Tallinn, and the analytic curve that was obtained from linear regression of this measurement using a quadratic frequency dependence.

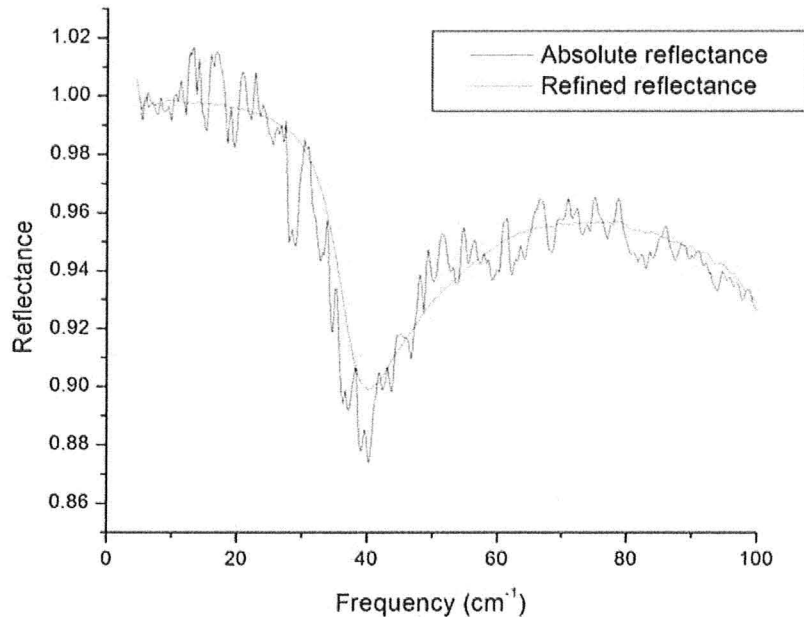


Figure 22 Absolute Reflectance and Refined Reflectance at 3 K.

The black curve was the measured result for absolute reflectance at 3 K measured by the group in Tallinn. The refined result using the parabolic fit at 20 K (P) and the measured thermal reflectance at 3 K (t_3) is shown by the red curve. The use of this analytic method showed a significant decrease in the noise of the reflectance curve.

The correction to the constant in the reflectance fit might be explained by an error in the experiment that might cause a 1% shift in the refined absolute reflectance (1.00 compared to 0.99). Since electron-electron scattering is known to behave as ω^2 (Ashcroft and Mermin), the quadratic frequency dependence suggests that this could be a large contribution to the absorption at low frequencies. Further investigation into the fitting method and into the expected contributions of electron-electron scattering would be an excellent starting point for future work.

The refinement method was used to calculate the absolute reflectance between 10 and 100 cm^{-1} from the thermal reflectance data (10 – 200 cm^{-1}) provided by Dr. Nagel (2010). The 3 K absolute reflectance, R_3 , was used to calculate the absolute reflectance at 20 K, R_{20} (using the 3 K thermal reflectance t_3 : $1/R_{20} = t_3/R_3$) between 100 and 200 cm^{-1} . The thermal reflectance for each temperature between 3 and 25 K was multiplied by R_{20} to obtain the absolute reflectance spectra for each temperature. The 20 K absolute reflectance was fit with an analytic curve obtained by a linear regression (P), and this analytic curve was multiplied with the thermal reflectance at each temperature between 10 and 100 cm^{-1} to reduce the noise in that region. That is, using the data provided by Dr. Nagel, the absolute reflectance was refined between 10 and 100 cm^{-1} , and joined with the absolute reflectance recovered from the thermal reflectance between 100 and 200 cm^{-1} , at each temperature, shown in Figure 20. These spectra were joined with the 25 K absolute reflectance between 250 – 38,000 cm^{-1} (measured by our group and calculated in Section 5.2) to obtain reflectance spectra in a frequency range from 10 to 38,000 cm^{-1} (the large frequency was required for Kramers-Kronig analysis discussed in Section 5.2). The optical conductivity was calculated from the refined data, using the method discussed in Section 5.2, and is shown in Figure 21.

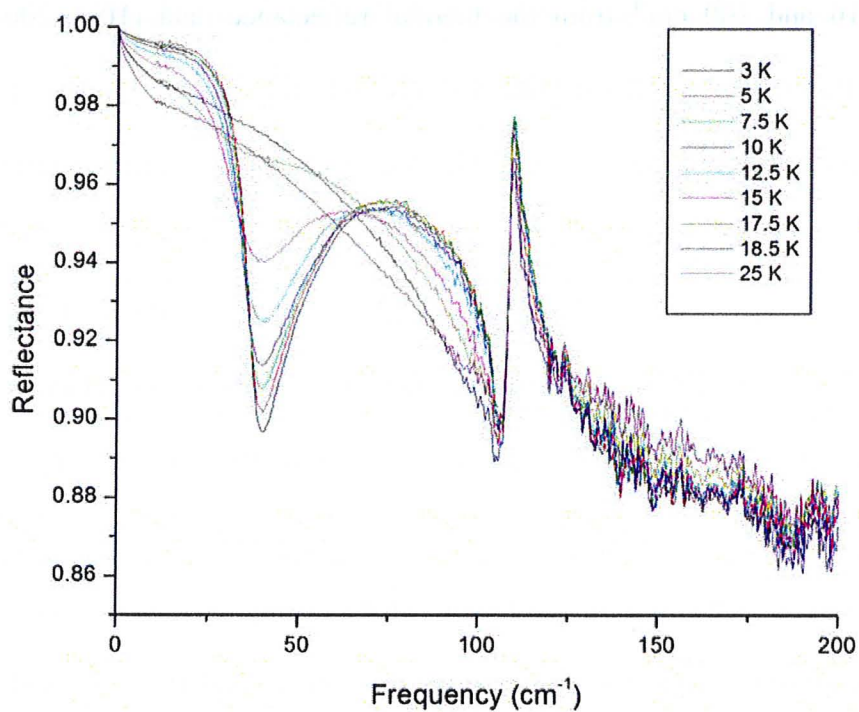


Figure 23 Refined absolute reflectance

Using data provided by Dr. Nagel (2010), refined in the 10 – 100 cm^{-1} frequency range, the Hagen-Rubens approximation was used to extrapolate the reflectance below 10 cm^{-1} .

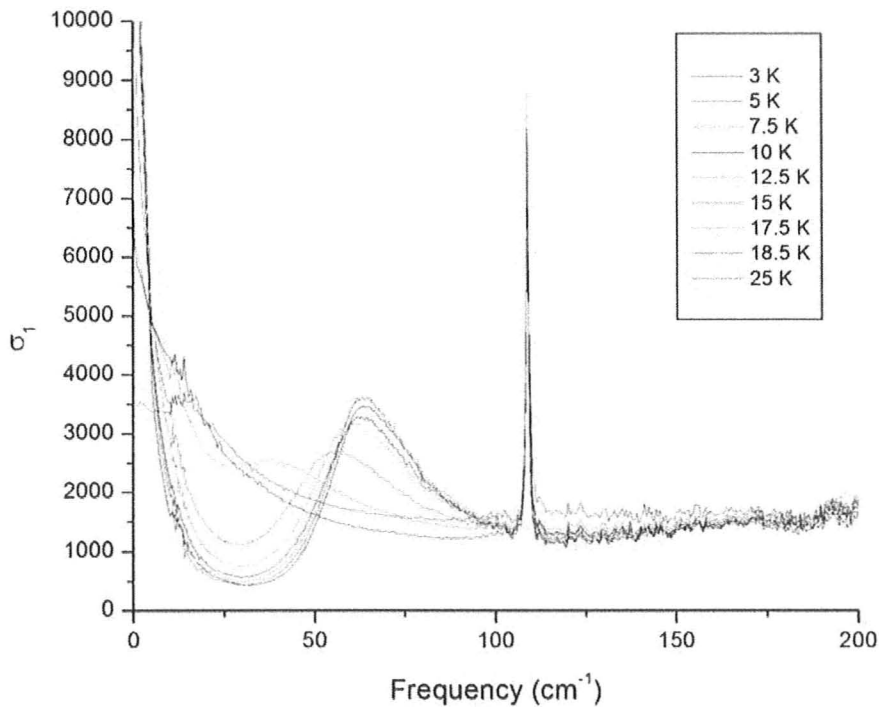


Figure 24 Optical conductivity calculated using the refined absolute reflectance

Using data provided by Dr. Nagel (2010), refined in the $10 - 100 \text{ cm}^{-1}$ frequency range. The single peak in conductivity at 60 cm^{-1} and the minimum at 30 cm^{-1} are attributed to the HO phase but no additional features are seen in these spectra below 100 cm^{-1} . The peak at 110 cm^{-1} is caused by a phonon (Bonn *et al.*, 1988)

The same behaviour seen by Bonn *et al.* (1988) is seen in Figure 25. A peak at 40 cm^{-1} appears at 17.5 K and shifts upward in frequency as temperature decreases to 10 K , and remains constant at 60 cm^{-1} between 7.5 and 3 K . a narrowing of the peak is seen with decreasing temperature as well. The additional features near 60 cm^{-1} that appeared in the thermal reflectance shared by Lobo

(2010) and Digiori (1997) do not appear in these refined data. The sharp peak at 110 cm^{-1} is a phonon mode (Bonn *et al.*, 1988).

5.2 Absolute Reflectance

The absolute reflectance of a material can be used to calculate properties such as the optical conductivity. It was calculated using my data as:

$$(5.1) \quad R = \frac{S/M}{S_c/M_c} C * \frac{M'}{M_c'}$$

Where S is the averaged reflectance measurement of the sample at some temperature T , M is the measurement of the reference, S_c is the measurement of the coated sample, M_c is the measurement of the reference mirror after the evaporation process, and C is the known spectrum of the coating material at or near T . The correction term M'/M_c' is the ratio of the reference mirror at room temperature just before and just after the evaporation, it accounts for any changes that may occur if some of the coating got on the reference mirror. The ratio of the sample to reference is taken in order to account for any drift or changes in the measurements during the collection of measurements at each temperature, as opposed to taking the ratio of the sample before and after coating.

The absolute reflectance without coating correction C was calculated using a Matlab program written by Jesse Hall. The coating correction had to be calculated separately since the gold and aluminum spectra used were not measured at the

same frequency points. A Fortran program written by Charles Porter and provided by D. Tanner at the University of Florida (Porter and Tanner, 2010) was used to “compare” (cmp.exe) the reflectance from Matlab calculations with the reflectance file of the coating. The absolute reflectance at 12.5 K, 25 K, 50 K, 100 K, 200 K and 300 K are shown in Figure 20.

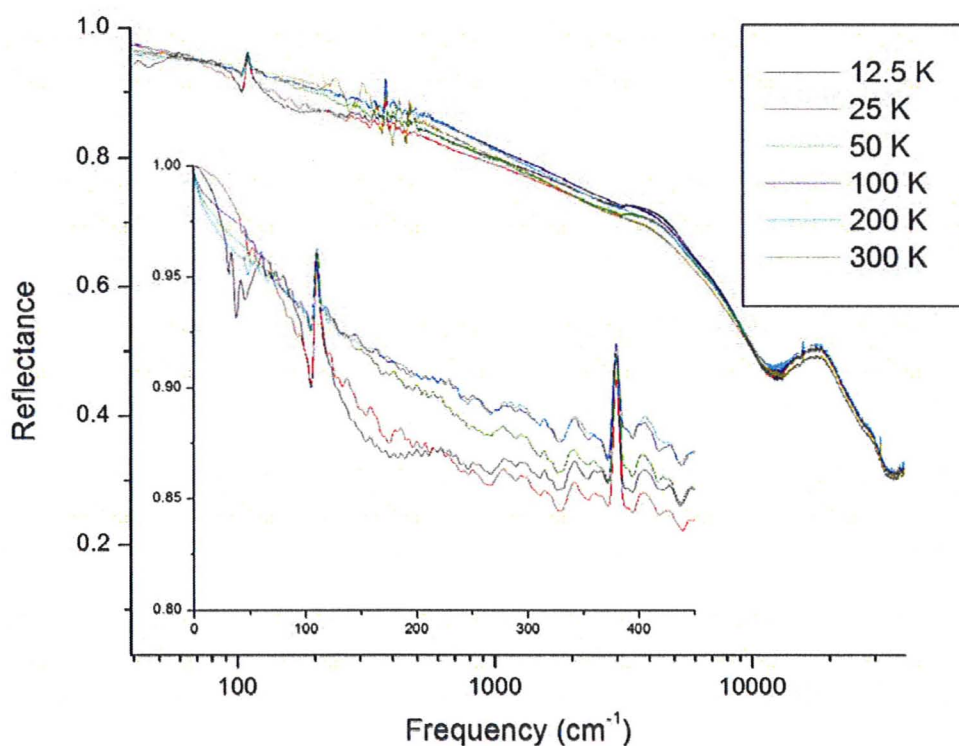


Figure 25 Absolute reflectance URu_2Si_2

The reflectance measured using the new spectrometer system in the frequency range from 25 – 38,000. The spectra at 12.5 K and 25 K were extrapolated between 0 and 25 cm^{-1} at low temperature using a ω^2 approximation, and at higher temperatures using a Hagen-Rubens approximation ($\omega^{1/2}$). The HO minimum in reflectance is seen at 40 cm^{-1} . Inset shows low frequency reflectance, 0 – 450 cm^{-1} .

The absolute reflectance shown in Figure 26 displays two large phonon peaks at 110 cm^{-1} and 380 cm^{-1} , and a gap at 40 cm^{-1} associated with the HO phase, all of these features were observed in earlier work (Bonn *et al.*, 1988). The 12.5 K and 25 K absolute reflectance spectra show the parabolic behaviour discussed in Section 5.1, and the 50 – 300 K data do not. The 4 K bolometer data was very noisy as seen in the 210 to 500 cm^{-1} spectral range. This spectral region was reduced from its usual range of 35 – 600 cm^{-1} to bridge the gap between the FIR data from the 1 K bolometer and the MIR data. The noisiness of the data made it difficult to join with the MIR data by averaging over the region of overlap between them, for this reason there is an artificial shoulder in the absolute reflectance near 500 cm^{-1} . Above 450 cm^{-1} the spectra should not display any temperature dependence (Bonn *et al.*, 1988) and when the individual absolute reflectance spectra at each temperature were plotted in their individual spectral ranges, no temperature dependence was seen for the MIR and NIR spectral ranges (the UV was only measured at room temperature). The spectra measured in the MIR and in the FIR matched to within 1%. At 3300 cm^{-1} a shoulder appears, in the MIR data near the expected ice absorption peak. The peak behaviour of this shoulder diminishes above $\sim 180\text{ K}$ (the sublimation temperature of ice in a vacuum; CRC handbook, 1952), but the shoulder remains.

5.3 Optical Conductivity

Much of the physics behind the analysis of the reflectance to obtain the optical scattering rate is discussed in many textbooks and articles (Kittel, 1976, Ashcroft and Mermin, 1976, Yang, J. 2005); only the essential equations are discussed here.

The majority of the data analysis performed after determining the absolute reflectance, R_T , was done using the Fortran programs written by Charles Porter. They included a program for Kramers-Kronig analysis to determine the phase factor, θ , and a conductivity program to calculate the optical conductivity, σ_1 from the absolute reflectance and the phase factor.

The Kramers-Kronig relation is applied in optics to calculate the phase factor, θ , – the imaginary term required for the complex reflection coefficient $r = \sqrt{R}e^{i\theta}$ where R is the measured absolute reflectance:

$$(5.2) \quad \theta(\omega) = \frac{\omega}{\pi} \int_0^{\infty} \frac{\ln R(\omega') - \ln R(\omega)}{\omega^2 - \omega'^2} d\omega'$$

This analysis required that the R data be extrapolated to zero frequency at low frequencies and to infinity at high frequencies. The spectral range that was measured was $25 - 38000 \text{ cm}^{-1}$ and different models were used to extrapolate the spectra at the extreme high and low frequencies. The frequency dependence of the reflectance was modelled for the different spectral regions and behaviours of the material: for a metal in the low frequency range ($<25 \text{ cm}^{-1}$) the Hagen-Rubens approximation was used ($R = 1 - A\omega^{1/2}$), that is for measurements at $T = 50 - 300$

K. As discussed in Section 5.1, the low temperature, low frequency measurements were extrapolated using a two-liquid model ($R = 1 - A\omega^2$). For the high frequency extrapolation for all of the measurements, a free charge carrier model was assumed ($R = \omega^{-4}$).

From the absolute reflectance, R , and the phase factor, θ , the complex reflection coefficient, r , can be expressed in terms of the complex index of refraction:

$$(5.3) \quad r = \frac{n + i\kappa - 1}{n + i\kappa + 1}$$

The real and imaginary indices of refraction are then given by

$$(5.4) \quad n = \frac{1 - R}{1 + R - 2\sqrt{R} \cos \theta} \quad \kappa = \frac{-2\sqrt{R} \sin \theta}{1 + R - 2\sqrt{R} \cos \theta}$$

Using the complex index of refraction, the complex dielectric constant is given by $\epsilon_1 + i\epsilon_2$.

$$(5.5) \quad \tilde{N} = n + i\kappa = \sqrt{\epsilon_1 + i\epsilon_2}$$

This can be used to find the real (σ_1) and imaginary (σ_2) parts of the optical conductivity, where $\epsilon_1 = n^2 - \kappa^2$, $\epsilon_2 = 2n\kappa$, and $\epsilon_\infty = 1$

$$(5.6) \quad \tilde{\sigma} = \sigma_1 + i\sigma_2 = \frac{\omega}{4\pi} \epsilon_2 + i \frac{\omega}{4\pi} (\epsilon_\infty - \epsilon_1)$$

Using these equations, the optical conductivity was calculated by a Fortran program, rph2s.exe from the absolute reflectance and phase factor data output by the KK.exe Kramers-Kronig analysis program. The real part of the optical conductivity is shown in Figure 21.

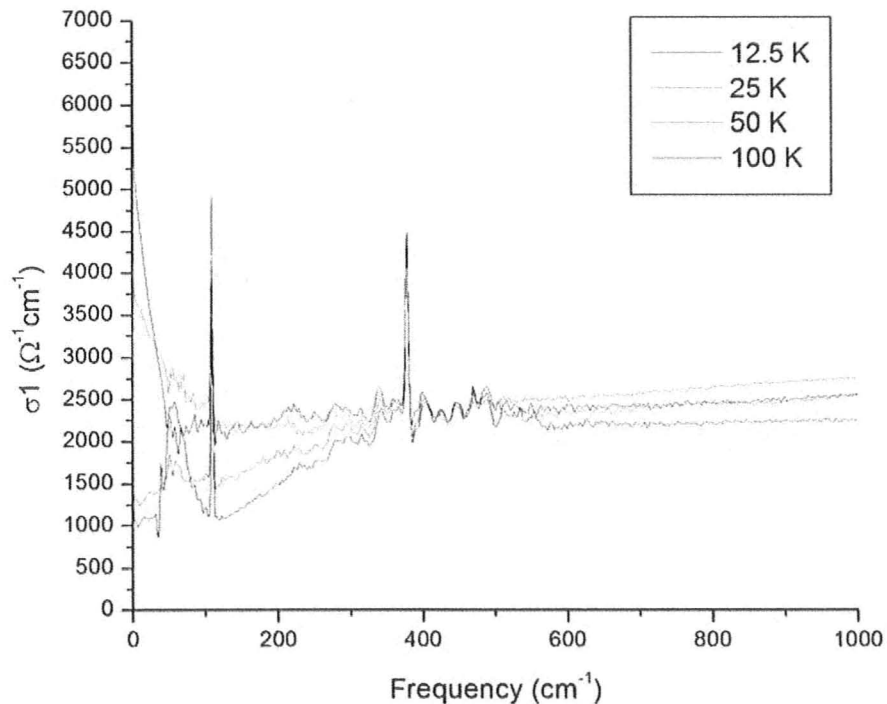


Figure 26 URu₂Si₂ Optical conductivity

Optical conductivity calculated from measurements made on the new spectrometer system. The 110 cm⁻¹ phonon peak was seen here, and the peak at 60 cm⁻¹ attributed to the HO phase at 12,5 K (below T₀ = 17.5 K). The data was normalized to the phonon amplitude by averaging the peak amplitude of the four data sets and multiplying the data by a normalization factor determined by the ratio of the average amplitude to the amplitude of the peak.

The optical conductivity highlights the separation of the 12.5 K and 25 K data from the 50 K data, indicating that the electron-electron contribution is not related to the coherence temperature T_c = 70 K. The strong phonon peaks at 110 and 380 cm⁻¹ are clearly visible, and the low frequency gap in the 12.5 K optical conductivity due to the HO phase is also distinct. There is a 5% difference in frequency between the peak seen here in the calculations from the measurements

done using the improved equipment at McMaster and the peak at 60 cm^{-1} seen in the 12.5 K optical conductivity that was calculated using the refined data from Dr. Nagel, seen in Figure 21. The peak should appear at 40 cm^{-1} at 17,5 K, and as temperature decreases, the peak shifts upward in frequency – this is why it appears at 60 cm^{-1} in the conductivity calculated from our measurements.

5.4 Fermi Liquid Behaviour

The frequency-squared (ω^2) behaviour can be explained using Fermi liquid theory, where the scattering rate is given by

$$(5.7) \quad 1/\tau = A'(\omega^2 + (\pi T)^2)$$

where A' is a constant. The scattering rate can be written in terms of the frequency dependent optical conductivity, and the plasma frequency ω_p .

$$(5.8) \quad 1/\tau = \frac{\omega_p^2}{4\pi} \frac{\sigma_1}{\sigma_1^2 + \sigma_2^2}$$

Using the relation for resistivity and complex conductivity $\rho_1 = \frac{\sigma_1}{\sigma_1^2 + \sigma_2^2}$, the

coefficient The constant, A' , can be determined by

$$(5.9) \quad A'(\omega^2 + (\pi T)^2) = \frac{\omega_p^2}{4\pi} \rho_1$$

$$(5.10) \quad A' \frac{4\pi}{\omega_p^2} = \frac{\rho_1}{\omega^2 + (\pi T)^2} = \frac{\rho_1 / \pi^2}{\omega^2 / \pi^2 + T^2}$$

We define

$$(5.11) \quad A = \pi^2 A' = \frac{\rho_1}{\omega^2 / \pi^2 + T^2}$$

At zero frequency, the coefficient is expressed in terms of resistivity and temperature.

The constant A can be determined using DC resistivity measurements (at zero frequency), or by optical conductivity measurements. The DC resistivity reported by Levallois *et al.* (shown in Figure 23) at 25 K was $160 \mu\Omega\text{cm}$, resulting in $A = 0.26 \mu\Omega\text{cmK}^{-2}$.

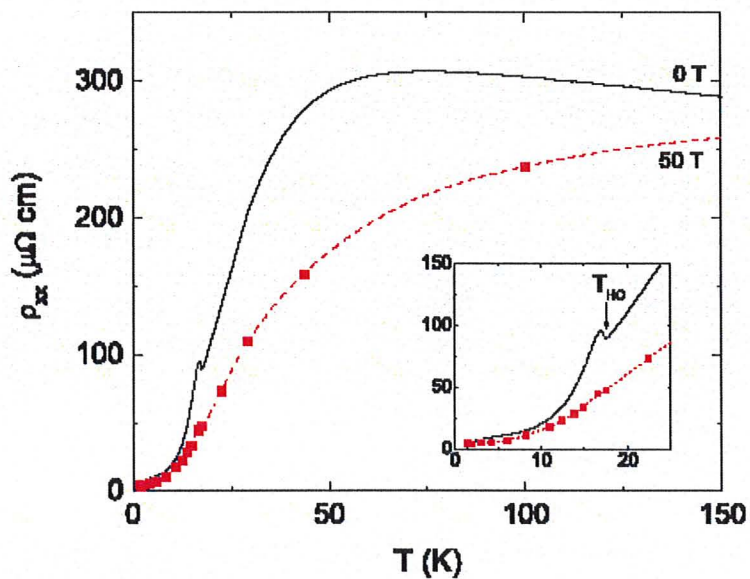


Figure 27 DC resistivity at zero magnetic field and at $B = 50 \text{ T}$ (Levallois *et al.*, 2009)

The constant A was also determined using the optical conductivity calculated from the refined absolute reflectance, from measurements shared by Dr. Lobo's group (2010) and from our group's measurements made using the new

spectrometer system. The results are summarized in Table 4. It can be seen from the good agreement of the A values obtained from transport where $A = 0.26 \mu\Omega\text{cmK}^{-2}$ and the optical values of 0.21, 0.23 and 0.23 $\mu\Omega\text{cmK}^{-2}$, all in reasonable agreement with one another, that the low frequency scattering at 20 K in the normal state above the HO transition in this material is well described by Fermi liquid electron-electron scattering. The constant is an estimate of the strength of the electron-electron scattering, the elastic scattering rate and bosonic excitations where neglected in the derivation of A .

Table 4 Fermi liquid parameter calculated using optical conductivity

Group	Temperature (K)	Frequency (cm^{-1})	σ_1 ($\Omega^{-1}\text{cm}^{-1}$)	σ_2 ($\Omega^{-1}\text{cm}^{-1}$)	A ($\mu\Omega\text{cmK}^{-2}$)
Lobo	25	100	1752	257	0.21
Nagel (refined)	25	100	1577	-120	0.23
Timusk	25	100	1474	139	0.23

6 Conclusion and Continued Work

A single crystal URu₂Si₂ sample was measured from 25 – 38,000 cm⁻¹ at temperatures between 10 and 300 K on a new sample stage system. The sample system was based on a translating stage that held a liquid helium flow cryostat to which the sample holder was attached. By having the samples directly on the cold finger of the cryostat, temperatures as low as 10 K were achievable. The sample system could hold up to three samples and one reference, each as large as 6 mm in diameter. The sample chamber assembly included an evaporator chamber for *in situ* evaporation of a reference material such as gold or aluminum onto the samples in order to account for surface irregularities (Homes *et al.* 1993).

The thermal reflectance was measured, using the improved equipment setup, at six temperatures between 10 and 20 K and compared to measurements from collaborators in Estonia (Nagel, U., 2010) and France (Lobo, R. 2010). The thermal reflectance data provided by Dr. Nagel was used to test a curve smoothing technique which resulted in a model of the absolute reflectance below 100 cm⁻¹ at temperatures between 3 and 25 K. The model was constructed using a linear regression of the absolute reflectance at 20 K. The optimized parameters gave the equation $P = 0.98716 - 8.0279E-6 * \omega^2$, with a regression coefficient of 0.8417, indicating that over 84% of the variability of the data was accounted for

by the model. The ω^2 behaviour in the refinement model was attributed to electron-electron interactions. The thermal reflectance at 3 K ($t_3 = R_3/R_{20}$) was multiplied by the best fit parabola to extract the absolute reflectance at 3 K (R_3). The refined absolute reflectance was compared to the measured absolute reflectance and found to have a standard deviation of ± 0.011 . Accounting for elastic scattering and bosonic excitations would result in a better fit to the unrefined data.

The strength of the electron-electron interactions uncovered by the investigation of the refining method was estimated using the DC resistivity published by Levallois *et al.* (2009) and found to be $A = 0.26 \mu\Omega\text{cmK}^{-2}$. It was also determined to be $0.21 \mu\Omega\text{cmK}^{-2}$ using the data shared by Dr. Lobo (2010), $0.23 \mu\Omega\text{cmK}^{-2}$ using Dr. Nagel's data, and $0.23 \mu\Omega\text{cmK}^{-2}$ using the measurements made using our new spectrometer system.

The refinement method was applied to the absolute reflectance spectra provided by Dr. Nagel between 3 and 25 K, and the optical conductivity was calculated. The refined data showed a gap at 40 cm^{-1} that opened at 17.5 K, which sharpened and shifted up in frequency as temperature was decreased to 7.5 K where it remained unchanged at 63 cm^{-1} as temperature was decreased to 3 K. No features aside from the single peak associated with the hidden order phase were observed in the optical conductivity calculated using the refined absolute reflectance.

The absolute reflectance was calculated from reflectance spectra measured using the new sample stage assembly (by our group in the Timusk lab), at six temperatures between 12.5 and 300 K. The absolute reflectance at 12.5 K showed a gap near 40 cm^{-1} associated with the HO transition. Improvements can be made to this reflectance by refining the merging and averaging of the regions of spectra between the spectral ranges that were measured. The 4 K bolometer data ($35 - 600 \text{ cm}^{-1}$) should be repeated. More measurements are required between 25 and 50 K to refine the estimate of the temperature at which the electron-electron interactions become a significant contribution to the reflectance.

From the absolute reflectance and the phase factor determined by the Kramers-Kronig analysis, the real part of the optical conductivity was calculated from our data for 5 temperatures between 12.5 and 200 K. A peak in the 12.5 K data at 57 cm^{-1} associated with the HO phase was observed, with a 5% difference from the peak frequency at 12.5 K using the refined data from Dr. Nagel (60 cm^{-1}). Further analysis to determine the optical scattering rate and bosonic spectral function are the logical continuation of this study.

List of References

- Ashcroft, N.W., and Mermin, N.D. *Solid State Physics*. Holt, Rinehart and Winston, Montreal. (1976)
- Basov, D. N., and Timusk, T. *Rev. Mod. Phys.* **77**, 721 (2005),
- Bonn, D. A., Garrett, J. D., and Timusk, T. *PRL* **61**, 1305 (1988)
- Carbotte, J. and Schachinger, E. Private communication. (2010)
- Cooper, R. A., Ph.D. Thesis: Optical Transport Properties of the High Temperature Cuprate Superconductor $\text{La}_{2-x}\text{Sr}_x\text{CuO}_4$. Univ. of Bristol (2009)
- Degiorgi, L., Thieme, St., Ott, H.R., Dressel, M., Grüner, G., Dalichaouch, Y., Maple, M. B., Fisk, Z., Geibel, C., Steglich, F. *Z. Phys. B* **102**, 367 (1997)
- Homes, C. C., Reedyk, M. A., Crandles, D. A., Timusk, T. *Appl. Opt.* **32**, 2976 (1993)
- Yang, J. M.Sc. Thesis: The doping and Temperature Dependence of Optical Properties of $\text{Nd}_{1-x}\text{TiO}_3$. McMaster Univ. Hamilton, Ontario (2005)
- Kittel, C. *Introduction to Solid State Physics, 2nd edition*. John Wiley and Sons, New York. (1976)
- Levallois, J., Behnia, K., Flouquet, J., Lejay, P., Proust, C. *EPL* **85**, 27003 (2009)
- Levallois, J., Lévy-Bertrand, F., Tran, M. K., Mydosh, J.A., Huang, Y.-K., van der Marel, D. ArXiv:1007.0583v1 [cond-mat.str-el] (2010)
- Lobo, R. Private communication. (2010)
- “BLT026 Specifications and Instructions” from McAllister Technical Services. <http://mcallister.com/blt026pg.html>, (August 2, 2010)
- Nagel, U. Private communication. (2010)
- Palmer, L.H., and Tinkham, M. *Phys. Rev.* **165**, 588 (1968)

Palstra, T. T. M., Menovsky, A. A., van den Berg, J., Dirkmaat, A. J., Kes, P. H., Nieuwenhuys, G. J., and Mydosh, J. A. PRL **55**, 2727 (1985).

Palstra, T. T. M., Menovsky, A. A., Mydosh, J. A. PRB **33**, 6527 (1986)

Porter, C., and Tanner, D., Data analysis programs,
<http://www.phys.ufl.edu/~tanner/datan.html> (2010)

“Pressure of Aqueous vapor: vapor pressure of ice” in Weast, C. W., ed., *CRC Handbook of Chemistry and Physics, 52nd Edition*, The Chemical Rubber Company Cleveland, Ohio, 1971.

Appendix A: Bruker Run Checklist

Success? Y/N

Date		
Operators		
File Path		
Window		
Beam splitter		
Detector		
	V_s	
	Operating time	
OPUS program		

Cone #	Sample	Evaporation	Signal Amplitude at RT
1			
2			
3			
4			

	Bolometer Transfer		Sample Cooling	
	Dewar Level	Wall Meter	Dewar Level	Wall Meter
Start:				
Finish:				
Total (L):				

Notes:

Sample Alignment (Day 1)

- Samples mounted on cones and sample holder
- Check alignment of reference (sample 1: stainless steel) Check alignment of light onto sample, reflected light on collection mirror and output spot.
- External alignment
- Make sure O-ring is in place for the cryostat-stage connection
- Make sure limit switch and controller connections are made, open labview controller programs
- Speed changed to 1000 and RC=50
- Internal alignment at collection mirror (adjust samples to hit same spot on the collection mirror)
- Internal alignment at output (adjust collection mirror) (place a piece of paper with crosshairs on the output port and make sure all spots line up at the output port)
- Attach radiation shield to cryostat
- Make sure cryostat-stage O-ring is in place, tighten nuts evenly, use rod (red taped) to make sure that the cryostat is centered in the sample chamber
- Once all hardware is together, attach detector, turn on appropriate light source if necessary*

ensure and get signal and check sample positions (relative positions) and record the number of steps between each one.

Evaporator Check (Day 1)

- Clean tungsten, make filaments
- Attach gold or (cleaned) aluminum, clean filament with acetone and kim-wipe
- Clean evaporator plate and collimators
- Connect filament to evaporator plate
- Attach collimators
- Electrical check (Black/White, Blue/Orange, Purple/Yellow and one from each pair to ground; adjust filament if it is grounded)
- Insert evaporator plate to box with O-ring, electrical check as before.
- Check O-rings for sample chamber-evaporator box and limit switch-evaporator box
- Attach limit switch and evaporator box to sample chamber

Hardware Check (Day 1)

- (optional) Check limit switch position visually with evaporator box on backwards and upside down
- Move stage up and down in large steps to see if any grinding or dragging occurs
- Attach window, Check its O-rings and secure stage to mounting bracket
- Electrical check of evaporators with all hardware in place.
- Connect temperature controller to cryostat, set temperature to 310K and make sure temperature rises
- Pump optics and sample chamber (overnight)

Optics Check (Day 2)

- Check reproducibility of samples (if they are not the same as before, try adjusting the positions up by a few thousand steps and rechecking until good reproducibility is found)

- Double check the relative positions and number of steps between samples
- Limit switch check

Landmark	Position	Number of steps to neighbour (up, down)
Sample 1		
Sample 2		
Sample 3		
Sample 4		
Limit Switch		

Transfer (Day 2)

- Measure Dewar level
- Record wall meter reading
- Blow dry He through transfer line
- Mark bottom of Dewar and liquid levels on transfer line with marker
- Insert Transfer line (Dewar end first, allow gas to flow before lowering cryostat end and tightening the nut 3-4 times. Allow gas to flow for ~1min before lowering the Dewar end into liquid)
- Connect and check return lines
- Check flow at flow meter, then turn to 0 at flow controller
- DO SCIENCE!

PID settings for Lakeshore controller

	50	200	300
P	20	50	100
I	40	20	10
D	100	100	100

	Beam splitter	Window	Detector	Evaporator coil
FIR (20-600 cm^{-1})	6 μm Mylar 50 μm Mylar	Polypropylene	1K bolometer	Gold
FIR (50-650 cm^{-1})	6 μm Mylar 50 μm Mylar	Polypropylene	4K bolometer	Gold
MIR (500-6000 cm^{-1})	KBr	KBr	77K MCT	Gold
NIR (3000-14000 cm^{-1})	UV/Ca	KBr	77K MCT	Gold
UV (12000-38000 cm^{-1})	UV/Ca	KBr	PMT	Aluminum

Appendix B: Cleaving layered materials

This method is best performed under a microscope, with good light and fresh gloves and a new razor. It can be used to “resurface” a material that has oxidized (on the scale of hours for $\text{Ba}(\text{Fe}_{1-x}\text{Co}_x)_2\text{As}_2$) (BFCA) or is scratched or otherwise un-useable.

Place the sample under a microscope, making sure that it allows room to manoeuvre. Look for an edge with terraces to help the razor get started. Grip the razor so that it is as flat as possible, too much of an angle to the sample will cause the layer that is being removed to crack, resulting in an impartial cleave and a hangnail flake on the surface. Hold the sample with a gloved finger and position the razor along the terraced edge of the crystal. Slide the razor into the sample a short distance, do not slice right through the sample as this could scratch the surface you want to use. The idea is to loosen the layers not cut through them; the action is similar to removing a Tupperware lid: loosen the corner and the whole lid comes off, ideally without having to lift all of the edges. The surface of the crystal will flex a little, but too much flexing and the flake will break. In some cases where the top flake is very thin, it may be transparent; thinner layers are harder to remove without breaking.

Once you have a small section of flake loosened from the surface, lift vertically with the razor to break the whole layer off of the crystal.

This also works with the sample glued or fixed to some surface, but it can be tricky to move the sample. One such cleave was successfully conducted with a

BFCA sample mounted on a sample cone after gold from an evaporation could not be removed from scratches in the surface.